Transient Disturbances in the Atmosphere and Ocean - their growth, transport properties and interaction with the general circulation

Nicholas M.J. Hall

1. INTRODUCTION

The governing equations of motion for the atmosphere and ocean are nonlinear. This means that the laws that determine the future state of either system depend on products of the system's state variables. This nonlinearity is responsible for the following phenomena:

- sensitive dependence on initial conditions: we can't predict the weather more than a few days ahead.

- difficulty in attributing cause: when a perturbation occurs, the question as to what caused it is often impossible to answer, or meaningless.

- asymmetry in response: the remote response to El Niño is not the exact opposite of the remote response to an equal and opposite 'La Niña'.

- scale interaction: the aggregate effect of small short lived systems plays an important role in the development of the system at larger scales over longer periods.

This final point on scale interaction is a linking theme in much of the work I have done in my career and that I present here in this monograph. This observation is at once trivial and profound. It is trivial because I have always worked with atmosphere/ocean dynamics, which is nonlinear and thus scale interactions are bound to be important. It is profound because this fact has a fundamental influence on the way we see the system, the difficulties we have in modelling it, the measurements we take and the problems we pose.

To start to formalise the effects of nonlinearity and scale interaction, consider a general state variable $\mathbf{\Phi}(x, y, z, t)$. $\mathbf{\Phi}$ is a state vector that defines the state of the system at a given moment. It contains variables such as temperature, pressure and velocity in some basis. A nonlinear law for the time development of the system can be written as

$$\frac{d\mathbf{\Phi}}{dt} = \mathbf{L}\mathbf{\Phi} + \mathbf{\Phi}^{\dagger}\mathbf{Q}\mathbf{\Phi} + \mathbf{F}(x, y, z, t), \tag{1.1}$$

where $\mathbf{L}$ and $\mathbf{Q}$ are matrices and $\mathbf{\Phi}^{\dagger}$ is the diagonal matrix whose leading diagonal consists of the elements of the column vector $\mathbf{\Phi}$. The first term in (1.1) is linear, the second quadratic. $\mathbf{F}$ is a forcing imposed externally on the system, or it can also represent processes not contained in the physical laws expressed by $\mathbf{L}$ and $\mathbf{Q}$. The dynamical nonlinearity contained in the second term is essentially advection, $-\mathbf{v}.\nabla q$ where $\mathbf{v}$ is velocity and q is the quantity being advected. Note that nonlinearity can also arise from other processes, for example the thermodynamics of moist air, or the behaviour of salt water under pressure, but here we will only consider advection. The advection term obviously involves the product of state variables $\mathbf{v}$ and q. It is part of the flux convergence, $-\nabla.\mathbf{v}q = -\mathbf{v}.\nabla q - q\nabla.\mathbf{v}$. Whether we are interested in flux convergence or advection depends on whether we consider q as point quantity like temperature or humidity or as the density of an integrated quantity like energy or total water content. Either way it is a quadratic term, and the essence of scale interaction is that when there is a product in the equation, any dual representation of the system (fast/slow, large/small) will result in one part of this dual representation influencing the other. To illustrate this consider the separation into long term mean (overbar) and deviation (prime):

$$\begin{aligned} \mathbf{v} &= \overline{\mathbf{v}} + \mathbf{v}', \\ q &= \overline{q} + q', \\ \overline{\mathbf{v}q} &= \overline{\mathbf{v}}\,\overline{q} + \overline{\mathbf{v}'q'}. \end{aligned} \tag{1.2}$$

The long term mean flux $\overline{\mathbf{v}q}$ is made up of the flux by the long term mean plus the aggregate effect over time of the fluxes by the transient disturbances. In this way transient systems feed back on climate. This principle also holds for any separation between scales. Often it amounts to the same thing because there are preferential scales of development for transient disturbances. Small scale phenomena are short lived and the larger scales develop more slowly. Thus in nonlinear systems like the atmosphere and ocean, small scale transient disturbances contribute to large scale transport of properties that define the large scale flow. In so doing they modify the large scale flow. In turn, the generation of the small scale systems depends on the state of the large scale, as energy and other dynamically conserved quantities are transferred between scales.

In the following sections I will present examples of this interaction and its consequences. Section 2 gives examples from dynamical oceanography. In section 3 we study the growth of transient systems in the atmosphere and how this depends on the large scale basic state. In section 4 we will look at the feedback effect of atmospheric transients, and along the way develop a simple GCM. Section 5 is a tour of past and future climates with an emphasis on transient disturbances in the atmosphere.

2. TRANSIENT DISTURBANCES IN THE OCEAN

2.1. Scale separation and parameterisation

In the ocean there is a clear separation of scales between the general circulation and the transient geostrophic eddy systems that are spawned by it. In dynamical terms, the oceanic general circulation is a very large scale phenomenon indeed, much larger than the global circulation of the atmosphere. This is because the ocean is relatively weakly stratified, and the Rossby radius of deformation NH/f, which defines the typical scale of geostrophic eddies, is of the order of 50-100 km, ten times smaller than in the atmosphere. A typical Gulf Stream ring system is thus much smaller than the Gulf Stream itself. From a theoretical point of view this separation is useful. However it poses severe difficulties for realistic modelling of the oceanic general circulation. To explicitly represent the transient eddies, a resolution of about 1/15 degree is required, which is beyond our current computer resources for large scale realistic simulations. The severity of the problem is a function of latitude. At 30^0N, the Rossby radius is about 40 km and the grid spacing of a state of the art 1/6 degree ocean GCM is 16 km. The eddies are not fully resolved but their presence is detectable on the model grid. At 60^0N the Rossby radius is 10 km, the model grid spacing is 9 km and the eddies are not represented at all. A 1/6 degree ocean GCM is thus not eddy resolving, but does achieve some degree of explicit representation of their presence. Such a model is known as 'eddy permitting'.

If the transient eddies are important for the general circulation, as stated in the introduction, then their large scale effect needs to be represented entirely in eddy non-resolving ocean models, and partially in eddy permitting ocean models. A parameterisation is sought whereby the effect of the unresolved eddies can be simulated in terms of resolved quantities. Diagnostics from eddy permitting GCMs are of interest to see what is already explicit and what needs to be parameterised. Fig. 2.1 shows the three dimensional divergence of transient eddy density flux in the North Atlantic from the CLIPPER OGCM (Treguier *et al*, 2001) taken from Hall (2004). Peak values are of the order of 10^{-7} kg/m^3/s, which corresponds a density change of 3 kg/m^3 over one year effected by the eddies. Negative (blue) values correspond to the creation of dense water by the eddy fluxes. Although there is much mesoscale noise, positive values are generally seen in along the Gulf stream, with a thin strip of negative values near the coast.

To parameterise the transient flux of density in terms of the mean density field, the usual approach is to assume some diffusive relationship between the mean density gradient and the flux. Gent and McWilliams (1990) recognised that this approach could be improved upon by also simulating the longer range transports of density effected by eddy induced secondary circulations. They rewrote the density advection equation in 'transformed Eulerian mean' form and defined an eddy transport velocity, or 'bolus velocity' $\mathbf{v}_b$, such that,

$$(u_b, v_b) = \frac{\partial}{\partial z}\left\{\frac{\overline{(u', v')\rho'}}{\overline{\rho}_z}\right\}, \qquad \nabla_3 \overline{\mathbf{u}'\rho'} = \nabla_3 \mathbf{u}_b \overline{\rho}, \tag{2.1}$$

so the transient eddy flux convergence is represented by the convergence of the flux of mean density by $\mathbf{v}_b$, which is shown in fig 2.1b. By construction, if the three dimensional bolus velocity is used to advect the mean density field, the resulting density tendency should be identical to the density tendency due to transient eddy density flux divergence. The assumption behind this identity is that there are no diabatic processes, i.e. there is no diapycnal flux of density. So the differences between figs 2.1a and 2.1b arise either from numerical noise, from the neglected vertical component of the bolus flux or from diabatic water mass creation. Clearly the main area of discrepancy is the area of wintertime dense water formation in the north east Atlantic. We have thus diagnosed a physical process as a residual, through a diagnostic consideration of transient fluxes. Nevertheless, the calculation is still quite noisy even with a twenty year simulation.

To create a true parameterisation a relationship must be defined between the long term mean flow and the transient fluxes. It is possible to diagnose a diffusivity from an eddy permitting

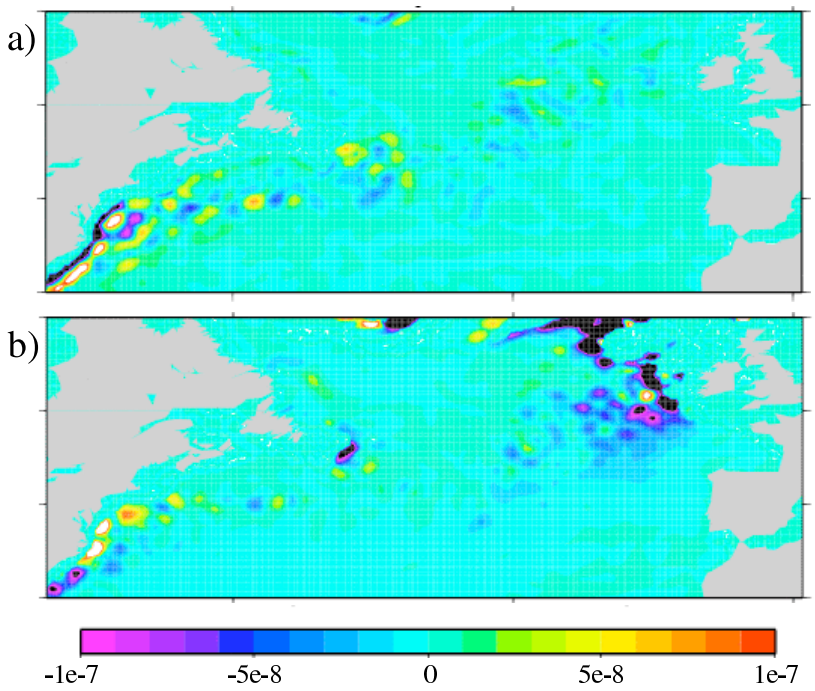

Figure 2.1. *Transient eddy diagnostics from a 20-year integration of an ocean GCM: (a) horizontal transient densitiy flux divergence, (b) advection of mean density by the horizontal bolus velocity. Units are kg* m^{-3} s^{-1}.

model integration, to see how the explicitly resolved transient fluxes are behaving. There are various ways to define the diffusivity, the simplest being in terms of the vector equation for the diffusivity κ

$$\overline{\mathbf{v}'\rho'} = -\kappa\nabla\overline{\rho}. \tag{2.2}$$

Here we present three possible approaches to calculating kappa from (2.2), they are

$$\kappa = -\frac{|\overline{\mathbf{v}'\rho'}|^2}{\overline{\mathbf{v}'\rho'}.\nabla\overline{\rho}}, \qquad \kappa = -\frac{\overline{\mathbf{v}'\rho'}.\nabla\overline{\rho}}{|\nabla\overline{\rho}|^2}, \qquad \kappa = -\frac{\nabla.\overline{\mathbf{v}'\rho'}}{\nabla^2\overline{\rho}}. \tag{2.3}$$

The first two definitions are mathematically equivalent and involve no approximation. The third definition is possibly more physically relevant, because it only considers divergent fluxes. It does however assume (for mathematical convenience) that gradients of diffusivity are aligned with gradients of density. If diffusivity varies slowly in the horizontal this assumption is reasonable. The diffusivity associated with each of these methods is shown in fig. 2.2. The first two methods are clearly not numerically equivalent. Method one gives excessively noisy results that go off the colour scale in the vicinity of zero contours whereas method two gives a smooth, if finely detailed field. It is the cross-gradient component of the density flux, appearing in the denominator of the first definition in (2.3), that is the source of the noise. The diffusivity for nondivergent eddy flux is significantly different again, but still less noisy. All three methods reveal a band of negative values of diffusivity south of the Gulf Stream, associated with upgradient density fluxes. These figures highlight the extreme difficulties associated with diagnosing a consistent

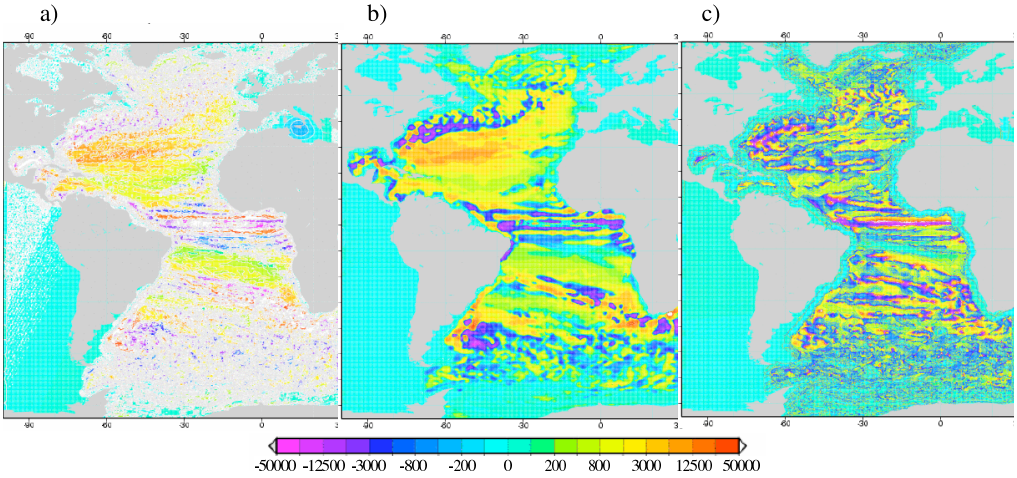

Figure 2.2. *Transient eddy density diffusivity coefficient ($m^2\ s^{-1}$) diagnosed using the three methods shown in equation (2.3).*

and universal parameterisation for transient eddy fluxes in the ocean, which is still essentially an unsolved problem.

2.2. Intergyre heat transport

One of the regions in which scale interaction in the ocean is most important is the North Atlantic. Northward transport of heat in this ocean basin accounts for a significant fraction of the global energy balance, and in this section some diagnostics from an eddy permitting ocean simulation reported by Hall*et al* (2004) are shown which break down this transport into components. In this way we isolate and quantify the various physical processes responsible. Two contrasting sections were taken across the North Atlantic subtropical gyre, shown in fig. 2.3. Here we concentrate on the section that follows the Gulf Stream and its seaward extension, and is parallel to contours of vertically integrated streamfunction (also shown in fig. 2.3). Heat transport crossing this section is referred to as the 'intergyre' transport. It corresponds to transport of heat between the subpolar and subtropical gyres perpendicular to the general circulation. An interesting question to ask about the intergyre transport is how does it respond to variability in the surface forcing (wind stress and heat flux). How much of the variability in heat transport is attributable to variations in surface forcing and how much is internally generated ?

Quite generally, the transport of heat across any given section can be broken down into components associated with spatial and temporal variations in the signal. Thus if the total heat transport across a section is $[\mathbf{v}T]$, there will be eight separate components that contribute to the total section transport:

$$[vT] = [\overline{v}][\overline{T}] + [\overline{v}^*\overline{T}^*] + [v'][\overline{T}] + [\overline{v}][T'] + [v'^*\overline{T}^*] + [\overline{v}^*T'^*] + [v'][T'] + [v'^*T'^*], \qquad (2.4)$$

where $[\,]$ and $*$ denote average along a section and departures from that average, and overbar and prime denote time average and departures from the time average. Of these terms, the last three are associated with transient disturbances and of these three only the last one contributes to the time mean transport across the section, although all three contribute to the variability.

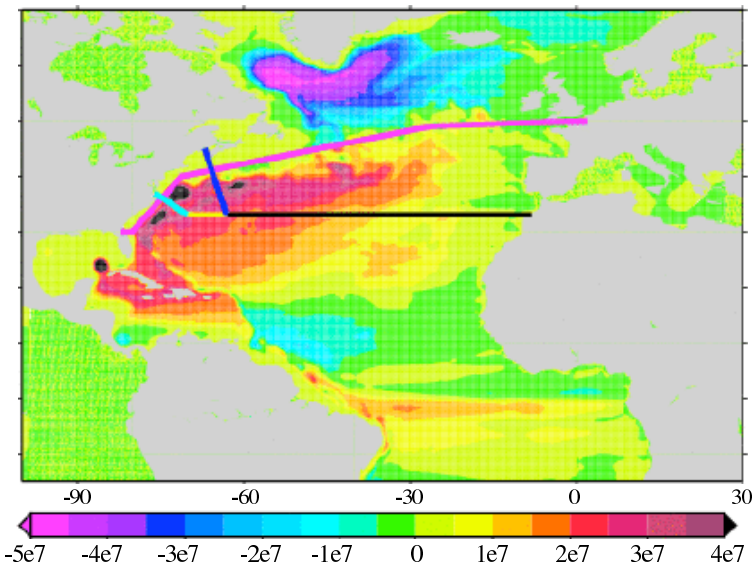

Figure 2.3. *Time mean barotropic streamfunction (m^2 s^{-1}) for an ocean model integration from 1980-1999 with sections used for the calculation of heat transport. The magenta section defines the intergyre transport.*

Timeseries for these diagnostics are shown in fig. 2.4 for two experiments. In one experiment a realistic surface forcing is imposed on the ocean model, and in the other the surface forcing is a repeated mean annual cycle, so that any interannual variability must be internally generated by the ocean model. The intergyre transport shows strong interannual variability but a weak annual cycle (in the experiment with the repeated annual cycle forcing, the interannual variability is weaker). About half the intergyre transport is due to transient disturbances, which also contribute strongly to the interannual variability. It turns out that the annual cycle in the transient terms cancels the annual cycle in the overturning components associated with Ekman transport (not shown). A large proportion of the interannual variability is attributable to an immediate Ekman response to changes in wind forcing. On the other hand it seems that the interannual variations in *transient* intergyre transport is quite independent of the surface forcing. Thus the component of the variability associated with transient oceanic disturbances is internally generated and difficult to link with features of the surface forcing.

In conclusion we can state that there are essentially two sources of interannual variability in heat transport: a simultaneous response to interannual variations in wind stress, and an internally generated component associated with transient oceanic disturbances that is independent of the surface forcing.

2.3. Isolated gyres and potential vorticity homogenisation

Under certain conditions, scale interaction in the ocean can have dramatic consequences for the large scale general circulation. The property of transient eddies to diffuse potential vorticity (PV) downgradient can shape the PV field at scales much larger than the scale of the eddies.

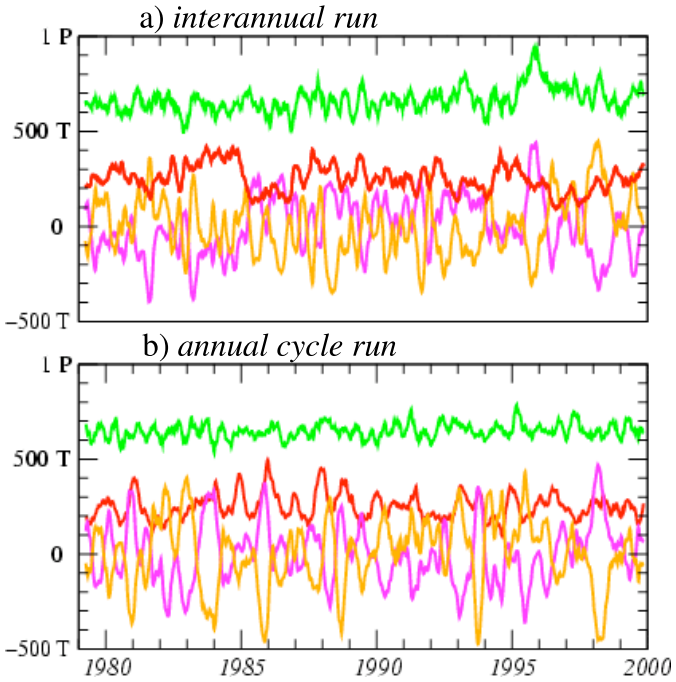

Figure 2.4. *Components of the intergyre heat transport for some of the terms listed in equation (2.4): total (green); transient eddies* $[v'^*T'^*]$ *(red); stream meander* $[v'^*\overline{T}^*]$ *(magenta) and isotherm meander* $[\overline{v}^*T'^*]$ *(orange). (a) Interannual run. (b) Repeated annual cycle run.*

Provided there is no other source or sink of PV, the result is a gyre scale region where all gradients have been eroded and where the PV is uniform. These conditions exist in 'unventilated' areas, isolated from the influence of surface forcing, in the abyssal flow beneath the Gulf Stream, on density surfaces that are too deep to come into contact with the surface further to the north. Since the PV determines the circulation, it follows that the circulation is shaped by the action of transients, which in turn are extinguished when there are no further PV gradients for them to grow on. The result is a laminar large scale flow regime for which theoretical solutions can be found, as was first shown by Rhines and Young (1982).

Boundary layer structures with uniform PV can be used as an archetype for the recirculation region associated with the eastward extension of the Gulf Stream. The vertical structure of such circulations was studied by Hall (1991) by solving the elliptic problem:

$$q = \beta y + \nabla^2 \psi + f_0^2 \frac{\partial}{\partial z} \left(\frac{1}{N^2} \frac{\partial \psi}{\partial z} \right), \tag{2.5}$$

where q is the imposed value of quasi-geostrophic potential vorticity and ψ is the horizontal streamfunction. A low value of q is assumed in the upper (thermocline) layers to simulate the weakly stratified 'mode' water found south of the Gulf Stream, and the homogenised abyssal value of q is set by the latitude of the Gulf Stream. The result is a vertically varying Fofonoff (1954) gyre where the extent of the abyssal flow is found by iterating to satisfy a no slip boundary condition at the southern limit. This provides the shape of the abyssal circulation. The latitudinal extent over which the circulation reaches the ocean floor has consequences for the total mass transport of the system. The solution is shown in figure 2.5.

The principal conclusions of this work are that the relative vorticity term (the second term

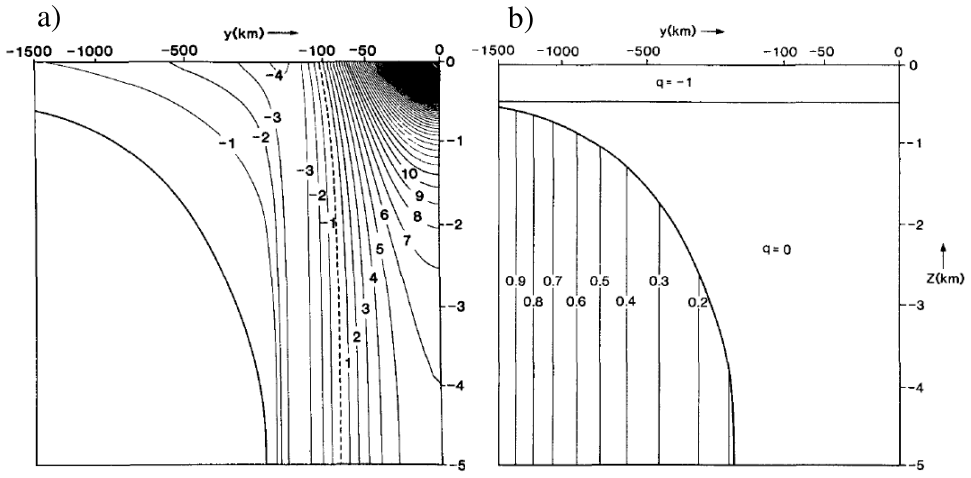

Figure 2.5. *Latitude - depth section for the abyssal flow icluding its depth penetration, based on inversions of idealised potential vorticity distributions. (a) Zonal current (cm* s^{-1}*), (b) imposed potential vorticity in units of* βy*.*

in (2.5)) is vital either to limit the vertical extent of the flow or to control its depth integrated structure, but that the vortex stretching term (third in (2.5)), although it disappears in the vertical integral, is dominant in magnitude, offsetting $q - \beta y$ over most of the gyre. The stronger the PV anomaly in the thermocline layer, the deeper the thermocline dips down, leading to a greater southward extension of the region where the currents reach the bottom, and a stronger recirculation.

3. THE GROWTH OF TRANSIENT DISTURBANCES IN THE ATMOSPHERE

3.1. Scale separation and the basic state

As mentioned in the introduction, the scale separation between geostrophic eddies in the atmosphere and the general circulation is less pronounced than in the ocean, being essentially limited by the size of the planet. Travelling weather systems associated with high and low pressure centres have a scale of the order of one thousand km and have lifetimes of the order of a few days. More slowly varying aspects of the atmospheric circulation such as the midlatitude jets or the large scale phenomena known as teleconnections (for example the 'North Atlantic Oscillation' or the remote response to El Niño) have scales of several thousand km and timescales measured in weeks to months. The separation between the two may be arbitrary. Nevertheless the associated physical processes are quite distinct and there are numerous studies showing how the shorter timescale transient disturbances are shaped by the changing background flow, and how in turn they feed back on longer timescales and influence the general circulation and the low frequency variability. In this section we will first discuss the concept of a 'basic state' and then show examples of perturbation studies that show how the basic state atmospheric circulation determines the structure of transient disturbances in the midlatitude 'storm track' regions and in the subtropical phenomenon of African easterly waves.

The growth of transient disturbances is often described in terms of perturbation theory. A fixed pattern of circulation called the 'basic state' is defined and used, together with the equations of motion, to predict the growth and structure of the most likely perturbation associated with this basic state. A desirable property of the basic state is that it resembles in some way a typical large scale state of the atmosphere, particularly during the growth of transient disturbances. Another more technical property of the basic state that is sometimes sought, is that it is itself a solution of the equations of motion. Using the notation from equation (1.1), such a basic state $\mathbf{\Phi}_0$ would satisfy

$$\mathbf{L}\mathbf{\Phi}_0 + \mathbf{\Phi}_0^\dagger \mathbf{Q} \mathbf{\Phi}_0 + \mathbf{F}_0 = 0, \tag{3.1}$$

where $\mathbf{F}_0$ is a steady radiative convective forcing. Introducing perturbations with subscript 1 (as in equation 1.2) and substituting into (1.1) we see that the perturbations $\mathbf{\Phi}_1$ will grow according to

$$\frac{d\mathbf{\Phi}_1}{dt} = \mathbf{L}_0 \mathbf{\Phi}_1 + \mathbf{\Phi}_1^\dagger \mathbf{Q} \mathbf{\Phi}_1 + \mathbf{F}_1, \tag{3.2}$$

where $\mathbf{L}_0$ is another matrix that depends on $\mathbf{\Phi}_0$ and includes both $\mathbf{L}$ and the advection terms involving the matrix $\mathbf{Q}$ and products of the basic state $\mathbf{\Phi}_0$ with the perturbation $\mathbf{\Phi}_1$. We say that $\mathbf{L}_0$ is the linearisation of the equations of motion about the basic state $\mathbf{\Phi}_0$. Equation (3.2) gives us a law for the growth and structure of transient disturbances to the basic state $\mathbf{\Phi}_0$, and equation (3.1) tells us that the form of $\mathbf{\Phi}_0$ is independent of those transient disturbances. Thus we have a well posed prediction problem, provided we can find a suitable structure for $\mathbf{\Phi}_0$. A basic state that truly satisfies (3.1) is, however, unlikely to be a realistic representation of an observable atmospheric general circulation. In reality the general circulation is heavily influenced by the action of transient disturbances. The terms in (3.2) are large and there is cancellation between them. None of these terms has a zero time-mean. This is because the basic state is unrealistic, so the perturbations $\mathbf{\Phi}_1$ must be large, with non-zero time mean. The interpretation of $\mathbf{\Phi}_1$ as a transient disturbance is therefore questionable. Furthermore, if $\mathbf{\Phi}_1$ is large, the nonlinear term in $\mathbf{\Phi}_1$ will also be large, so looking for linear solutions to (3.2) is of questionable relevance for the real atmosphere.

Another way of making the separation is to relax the condition that the basic state must be a solution of (3.1) and use a more realistic flow. Such a flow might be the time average circulation over a sufficiently long period (i.e. much longer than the lifetime of the transient disturbances under investigation). Using overbar and prime for time mean and perturbation

(as in 1.2), the equation for the development of transient disturbances becomes

$$\frac{d\boldsymbol{\Phi}'}{dt} = \mathbf{L}\overline{\boldsymbol{\Phi}} + \overline{\boldsymbol{\Phi}}^{\dagger}\mathbf{Q}\overline{\boldsymbol{\Phi}} + \mathbf{L}_M\boldsymbol{\Phi}' + \boldsymbol{\Phi}'^{\dagger}\mathbf{Q}\boldsymbol{\Phi}' + \overline{\mathbf{F}} + \mathbf{F}', \tag{3.3}$$

where $\mathbf{L}_M$ is the linearisation of the equations of motion about the time mean flow $\overline{\boldsymbol{\Phi}}$. Note that this time we cannot subtract out the non-perturbation terms because the basic state no longer satisfies the forced equations of motion independently and thus contributes to the perturbation tendency. We therefore need to ask how the basic state is maintained. The time mean of (3.3) gives

$$\mathbf{L}\overline{\boldsymbol{\Phi}} + \overline{\boldsymbol{\Phi}}^{\dagger}\mathbf{Q}\overline{\boldsymbol{\Phi}} + \overline{\boldsymbol{\Phi}'^{\dagger}\mathbf{Q}\boldsymbol{\Phi}'} + \overline{\mathbf{F}} = 0. \tag{3.4}$$

This equation contains an extra term compared to (3.1), the third term, which represents the systematic effect of transient disturbances on the mean flow. This is often referred to as the 'transient eddy forcing'. We will make extensive use of this idea in the next chapter. So the transients can no longer be viewed as evolving independently of the basic state, and we must acknowledge the fact that the development of the transients is determined not only by the properties of $\mathbf{L}_M$, but also by a time mean forcing effect, arising from the very transient disturbances that we are trying to simulate.

Both approaches to the separation between basic state and perturbation thus have their advantages and drawbacks. In what follows we use the latter approach, preferring to trust that by analysing a realistic flow we have chance of determining some relevant properties of the transient disturbances even if this approach does not represent a complete theory for their growth. In the next section we will use this approach to discuss the stability of the midlatitude general circulation and the structure of midlatitude transients.

3.2. Baroclinic modes and storm tracks

Having grappled with some philosophical and technical issues to do with scale separation, we now turn our attention to the physical mechanisms behind the growth of transient disturbances. It is universally understood that in the atmosphere these disturbances draw their energy from the steady jet structures, feeding on their horizontal and vertical shear (barotropic and baroclinic conversions respectively). The precise nature of the growth has been a subject of some debate in the literature. The traditional viewpoint is one of an unstable basic flow, on which modal structures grow exponentially, reach finite amplitude and decay by a saturation process, whereby nonlinear terms become important, allowing the perturbation to alter its structure and return its energy to the basic flow. This in turn sustains the basic flow against other forms of dissipation. This viewpoint dates back to the canonical instability studies of Charney (1947) and Eady (1949) (if PhD supervisors were parents, Eady would be my great grandfather). An alternative viewpoint arising from the work of Farrell (1982) holds that the basic flow is stable, there is no exponential growth, but there can still be transient growth for a limited time due to interference between a number of decaying modal structures. In a stable atmosphere, nonlinear saturation is not necessary to explain the decay of transient systems, but some external noise is needed to provide initial excitation for the perturbations.

Both theories have had some success in predicting features of the general circulation. On the one hand exponentially growing modal structures have been found that closely resemble observed perturbations. On the other hand the range of growth rates observed in the atmosphere suggests that non-modal growth is also important. Neither viewpoint represents a complete theory for transient disturbances, because the former does not address the problem of transient feedback on the basic state in a self consistent way, and the latter does not specify the origin of the initial disturbance. To choose between the two, some measurement must be made of the stability of a relevant basic state. In this case, the time mean flow is undoubtedly a useful reference. If the time mean flow is stable, that means modal growth is impossible and the latter theory is the more relevant for a general description of the transient variability. If the time

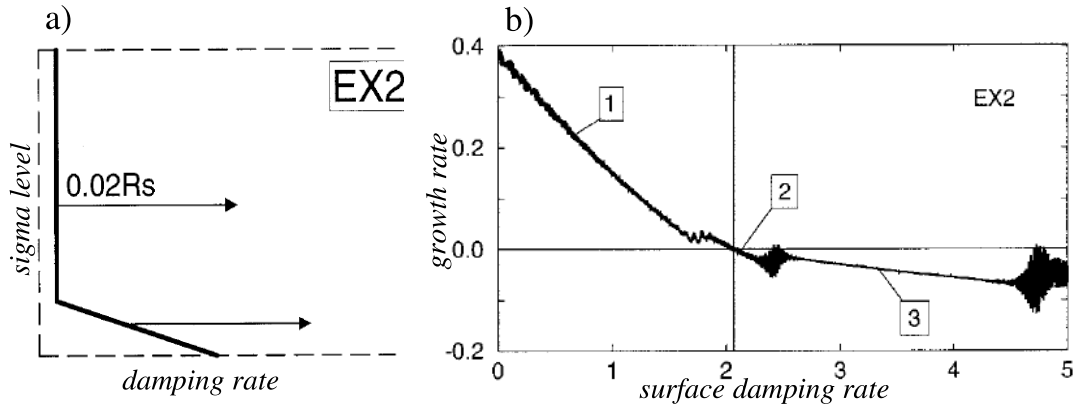

Figure 3.1. *Experiment with variable damping to establish stability of northern hemisphere wintertime atmospheric circulation. (a) Vertical profile of damping. (b) Growth rate of fastest growing linear normal mode as a function of increasing surface value of damping (d^{-1}).*

mean flow is unstable then it would be necessary to appeal to nonlinear processes to equilibrate the system, lending more credence to the traditional viewpoint at least as a partial theory.

This fundamental question was addressed directly by Hall and Sardeshmukh (1998). Using a primitive equation model, they studied the stability properties of the observed climatological flow under a range of parameters for low level turbulent transfer of momentum and heat. The problem is solved by using the model to solve the following equations

$$\frac{d\boldsymbol{\Psi}}{dt} = \mathbf{L}\boldsymbol{\Psi} + \boldsymbol{\Psi}^{\dagger}\mathbf{Q}\boldsymbol{\Psi} - \mathbf{L}\overline{\boldsymbol{\Phi}} - \overline{\boldsymbol{\Phi}}^{\dagger}\mathbf{Q}\overline{\boldsymbol{\Phi}}, \tag{3.5}$$

where $\boldsymbol{\Psi}$ represents the model state and $\mathbf{L}$ and $\mathbf{Q}$ now represent the primitive equation model. $\overline{\boldsymbol{\Phi}}$ is the observed time mean flow. The terms involving $\overline{\boldsymbol{\Phi}}$ can be viewed as a spatially varying but time-independent forcing, easy to find just by initialising the unforced model with $\boldsymbol{\Phi}_0$ and running it for one timestep. If the model is then initialised with $\boldsymbol{\Psi} = \overline{\boldsymbol{\Phi}} + \boldsymbol{\Psi}'$, and $\boldsymbol{\Psi}'$ is small, the subsequent development will satisfy the linear equation

$$\frac{d\boldsymbol{\Psi}'}{dt} = \mathbf{L}_M\boldsymbol{\Psi}'. \tag{3.6}$$

A long integration of (3.6) will eventually yield a shape preserving normal mode structure for $\boldsymbol{\Psi}'$. Care must be taken to occasionally rescale the perturbation to ensure that it remains small and the problem remains linear. The solution can be expressed as the eigenvalue relation

$$\mathbf{L}_M\boldsymbol{\Psi}' = (\sigma + i\omega)\boldsymbol{\Psi}'. \tag{3.7}$$

The mode grows at rate σ (or decays if σ is negative) and oscillates with angular frequency ω. For three dimensional basic states, $\mathbf{L}_M$ is generally asymmetric so the eigenvectors are complex. Two real spatial structures are therefore needed to fully describe the mode:

$$\boldsymbol{\Psi}'(\mathbf{x},t) = [\boldsymbol{\Psi}_A(\mathbf{x})\sin\omega t + \boldsymbol{\Psi}_B(\mathbf{x})\cos\omega t]\, e^{\sigma t}. \tag{3.8}$$

The mode thus cycles from structure $\boldsymbol{\Psi}_A$ to structure $\boldsymbol{\Psi}_B$, to $-\boldsymbol{\Psi}_A$, to $-\boldsymbol{\Psi}_B$ and back to $\boldsymbol{\Psi}_A$.

It is important to note here that the stability of the flow is not the same thing as the stability of the system. Any realistic midlatitude flow will be baroclinically unstable and will exhibit exponentially growing eigenmodes. However, with some prescription of low level drag,

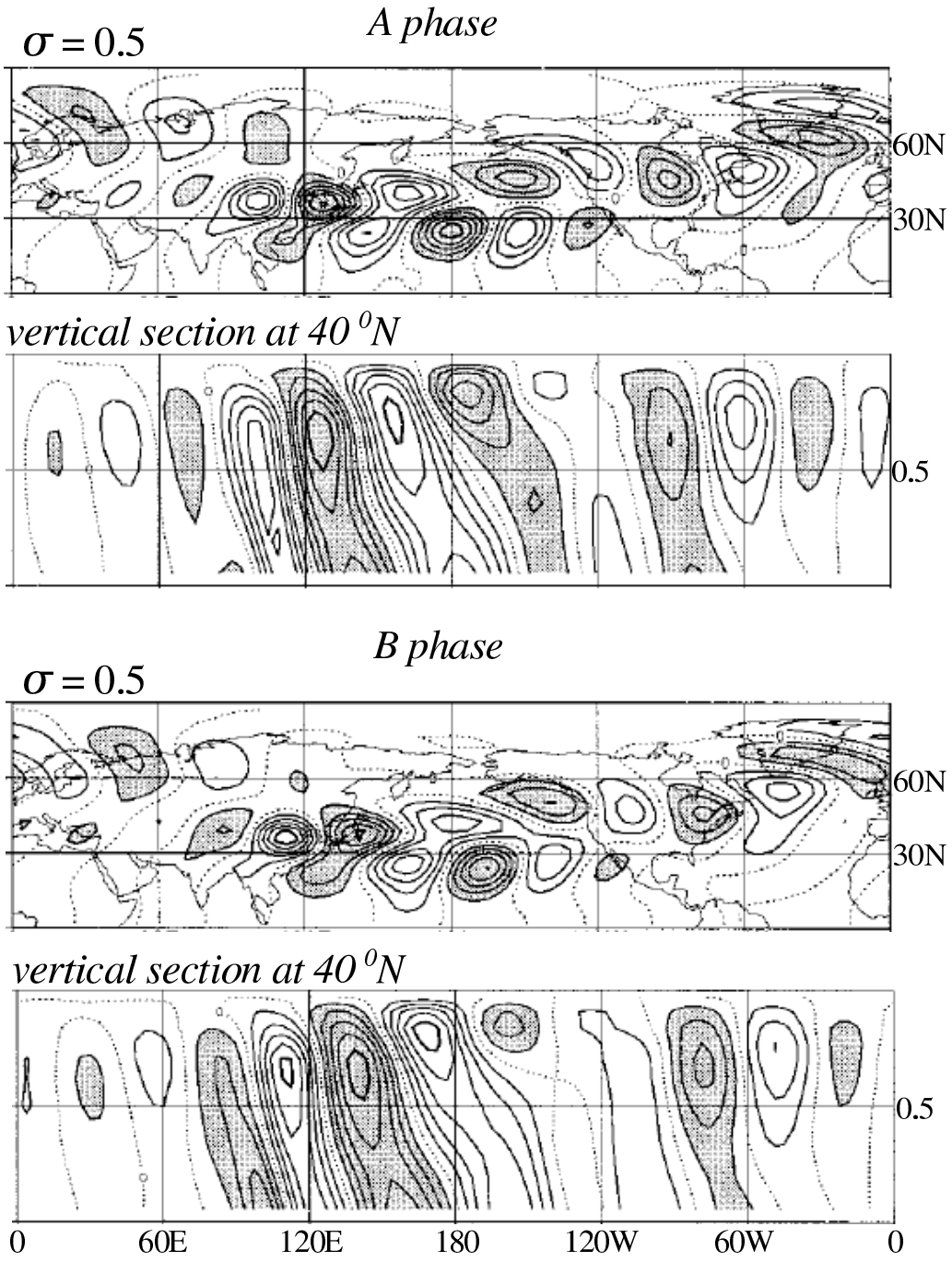

Figure 3.2. *Horizontal streamfunction at 500 mb and its vertical structure at 40^0N for the A and B quadrature phases of the dominant damped normal mode for the northern hemisphere wintertime flow. Damping at surface is 2 d^{-1}. Zero contour dotted, regions enclosed by negative contours shaded. Amplitudes are arbitrary.*

the system (basic flow plus laws of motion) can potentially be stabilised. Linear damping of momentum and temperature was used to simulate these boundary layer processes. In a series of experiments the coefficients were gradually ramped up, and the associated exponential growth rates of the fastest growing modes for the midlatitude circulation were diagnosed. The results are shown in fig. 3.1. With no damping, the time mean northern hemisphere flow is unstable and the fastest growing eigenmode has a growth rate of 0.4 days^{-1} (an e-folding time of 2.5 days). As the low level damping is increased, the growth rate decreases almost linearly to a point where the system is almost stabilised. This corresponds to region 1 on fig. 3.1. There is also a gradual modification of the associated modal structure. Then there is a jump, and another modal structure overtakes the previous one as the fastest growing (region 2). As damping is increased the neutral threshold is crossed (zero growth rate) and the fastest growing mode becomes the slowest decaying. Then there is another jump to a mode that has a completely different spatial structure which does not resemble midlatitude transients at all. Further increases in damping do little to further stabilise the system.

The key question is where does a realistic low level damping lie on the horizontal axis of fig. 3.1b ? Comparisons of this idealised study with drag-budget experiments with a GCM suggest that the neutral point in this experiment represents a reasonable prescription for the low level damping. We conclude that in a realistic setting, the time mean flow coupled with the laws of motion yield a neutral system. This conclusion puts theories that rely solely on exponential modal growth in some difficulty, although it does not entirely exclude this process as a relevant description of the structure of atmospheric transient phenomena.

The structure of our neutral mode (region 2 in fig. 3.1) is shown in fig. 3.2. A synoptic scale baroclinic wavetrain is revealed, initiating in the Asian jet and propagating across the Pacific and through North America. The vertical structure shows tilting against the shear implying baroclinic conversions of available potential energy to eddy energy, with upward propagation of the signal to a more barotropic (height independent) structure downstream. All of these features are realistic observed features of typical disturbances in the Pacific and Atlantic storm tracks, and it is interesting that they are reproduced here in a purely linear framework.

3.3. African easterly waves

Another well known and well studied phenomenon where this technique has recently led to interesting results is African easterly waves. These waves are intermittent perturbations that are observed over West Africa associated with the mid-tropospheric summertime African easterly jet. They have a period of 3-5 days and a spatial scale of about 3000 km. Over Africa they are of interest because of their interaction with convection and the associated precipitation, and as they migrate out over the Atlantic they are often associated with the genesis of hurricanes. The pioneering work in easterly waves combined considerations of the structure of the African easterly jet (Burpee, 1972) with observations from the GATE program (Reed et al, 1977). It was soon pointed out that the basic flow was dynamically unstable, and that the wave structure was consistent with energy conversions that can be associated with both barotropic and baroclinic instability. Since then, this mixed instability has been tacitly accepted as the source of easterly waves in observational and modelling studies alike. In this framework, the fact that the waves are intermittent in time may be ascribed to variations of the African easterly jet and how unstable it is. The modelling studies presented below call this point of view into question.

A recent paper by Kiladis *et al* (2006) uses time space filtering techniques to construct composite structures of a typical easterly wave from reanalysis winds and satellite cloud data. The spatio-temporal window associated with 3-5 day westward propagating features is used to filter outgoing long wave radiation (OLR) data, which is then used to construct one point correlation maps for various base points. The OLR is also correlated with dynamical fields from the reanalysis. Using several days lead and lag for the correlations, a picture emerges of a generic westward propagating signal with a typical structure illustrated in fig. 3.3.

Using the primitive equation model, Hall *et al* (2006) found the fastest growing mode associ-

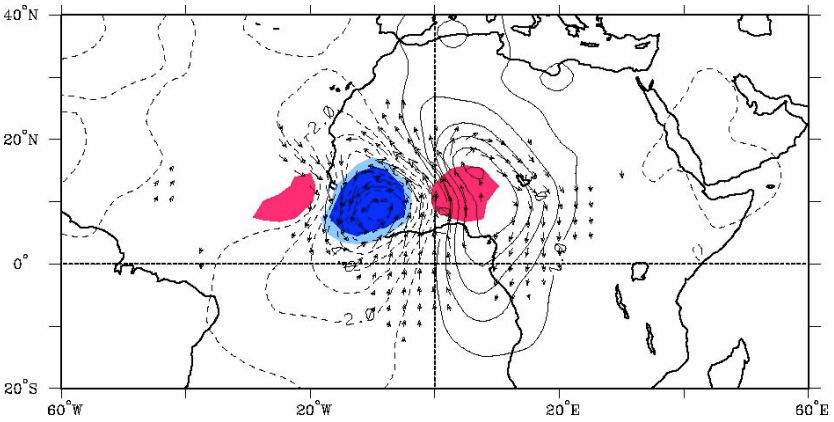

Figure 3.3. *Composite african easterly wave based on simultaneous correlations in space-time filtered OLR data at the base point 10^0 W, 10^0N. OLR and 850 mb streamfunction and winds are shown associated with an OLR anomaly at the base point of 40 W m^{-2}. Colouring shows OLR anomalies of 10 W m^{-2}; blue for increased convection, red for decreased convection. Streamfunction contours $2 \times 10^5 m^2 s^{-1}$, largest velocity vectors about $2ms^{-1}$.*

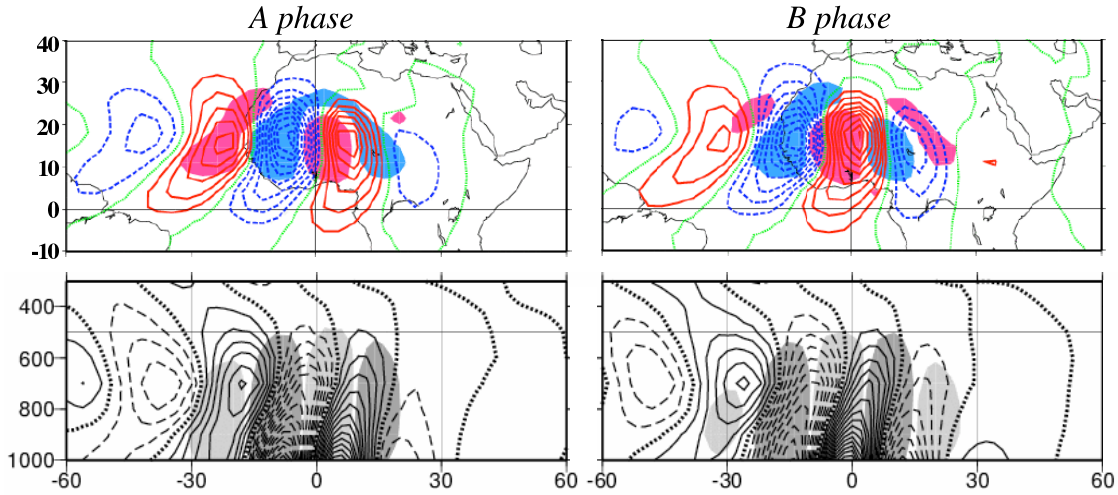

Figure 3.4. *Modal structures for African easterly waves showing horizontal structure at 850 mb and vertical structure along 15^0N. Contours show streamfunction (negative dashed) and colouring/shading shows dynamically consistent vertical velocity: blue/heavy for upwards and red/light for downwards. Amplitudes are arbitrary.*

ated with the summertime climatological circulation over west Africa. This is presented in figure 3.4. The similarities between figures 3.3 and 3.4 are remarkable. Both show a ridge-trough structure that is initiated around 20^0E and has its maximum intensity near the Greenwich meridian. The waves begin their lives at relatively low levels with a vertical structure consistent with baroclinic growth. They propagate upwards to the level of the mid-tropospheric jet, and downstream, as they leave the coast, they acquire a more barotropic backwards C shaped structure, implying transfer of kinetic energy from the jet to the waves. Unlike midlatitude

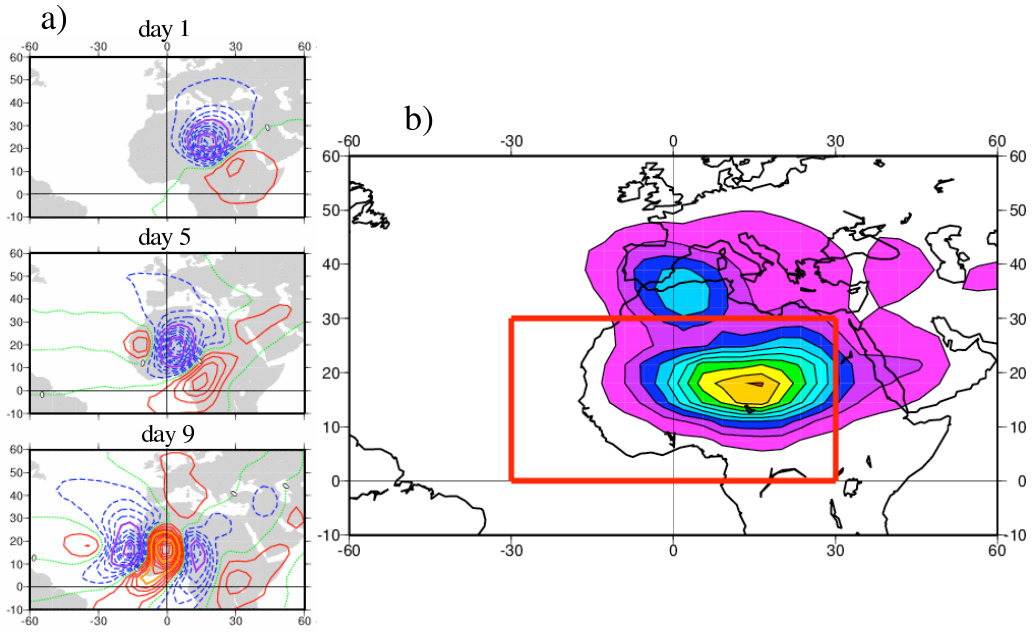

Figure 3.5. *(a) Time development of 850mb streamfunction reponse to a heat source placed on the Sudan-Chad border (25^0E, 12.5^0N) for one day. (b) Influence function for many heating experiments in which the position of the heating is varied. Contours show day-9 mean squared streamfunction response (averaged within the red box target area) plotted in the position of initial heating. Maxima indicate where heating is most effective in inducing a wave response in the target area.*

waves, they therefore feed off the jet throughout their lifecycle. The position of ascent in the waves is also of interest. In the observed composites the regions of enhanced convection (negative OLR anomalies) are situated in the northerlies over the continent, and in the trough off the coast. This variable phase relationship is exactly reproduced by the dynamical mode for the upwards vertical velocity. Hall *et al* explain this phase relationship in terms of vorticity advection in a modulated wave packet. The fact that the idealised dynamical mode resembles the observations suggests a dynamical origin for regions of favoured convection within the wave.

To produce the structure shown in fig. 3.4 some low level damping was included as described above. The strength of the damping was quite modest, about half as much as is needed to neutralise the midlatitude winter flow (see fig. 3.1). But it is enough to neutralise the easterly wave mode, which in fact decays slowly (without damping the growth rate is 0.25 d^{-1}, rather slower than a midlatitude storm track). It seems reasonable to conclude that the African easterly jet is effectively stable. If the traditional instability theory is in difficulty for the midlatitudes, it is surely dead and buried for the African jet. Even if the system were unstable, the jet is so short that there is scarcely time for a wave to develop from a small perturbation before it has propagated out of the jet exit.

How then are we to explain the intermittency of African waves ? Hall *et al* did further analyses based in the summertime mean circulation for 1988 and 1990, respectively very busy and very quiet years for easterly waves. The basic states are actually very similar, and the modes are stable in both cases. Intermittency of the stability of the flow seems an unlikely candidate to explain intermittency in the waves. Since the system is stable, a finite amplitude perturbation is needed to initiate a wave-like response. Once the system is perturbed, it will naturally resonate close to a modal structure after a few days, even if the mode is stable. This has been confirmed by initial perturbation experiments. Fig. 3.5a shows the time-dependent

response for such an experiment, in which a heat source was imposed for one day over the Sudan-Chad border. The initial response is a baroclinic heat low, but after several days the wave-like mode emerges, and eventually decays. A great many such experiments serve to reveal the most effective location for the initial perturbation, shown by the influence function in fig. 3.5b.

In summary, we have shown that dynamical modes based on the full three dimensional climatological flow can go a long way to explaining some of the observed features of African easterly waves. They also call into question the idea that the system grows through instability. Easterly waves are more likely to begin with a large perturbation to the east, possibly convective. They are then seen to organise convection downstream, with a complicated phase relationship.

4. TRANSIENT FEEDBACK, TELECONNECTIONS AND THE ATMOSPHERIC RESPONSE TO SST ANOMALIES

4.1. Transient forcing, the eddy budget and a simple GCM

There is a range of complexity for atmospheric models. The most complex is the general circulation model, which is a physically based comprehensive representation of all the dynamical and physical processes that make up the atmospheric circulation. GCMs can be realistic, useful for weather or climate prediction, but also difficult to diagnose and expensive to run. To concentrate on a particular mechanism in isolation, idealised models are used. These models are diagnosed in a rigourous way and a more complete and satisfying understanding can be achieved, but often at the expense of some degree of realism. Between these two extremes there is a class of model called a 'diagnostic model', where a limited number of processes is studied for the sake of simplicity and clarity, but the solution is also constrained in some way by observations, so that it is more realistic and relevant. In this chapter we will draw on the eddy budget concepts developed in the previous chapter to develop such a model: a GCM based only on dynamics and constrained by observations. This model will be applied to various problems in boundary forcing in the tropics and extratropics. One advantage of this type of study is the ease with which it can be placed in a hierarchy of studies, and this feature will be used to highlight the role of transient disturbances in shaping lower frequency phenomena.

The generic equation (1.1) shown in chapter one can be taken to represent the time development of the observed atmosphere. If we are to model this system, a model equivalent of (1.1) must be constructed in some way. Consider the model equation

$$\frac{d\mathbf{\Psi}}{dt} = \mathbf{L}\mathbf{\Psi} + \mathbf{\Psi}^\dagger \mathbf{Q}\mathbf{\Psi} + \mathbf{G}. \tag{4.1}$$

The only difference between (4.1) and (1.1) is that the state vector $\mathbf{\Psi}$ now represents the model state rather than the observed state $\mathbf{\Phi}$, and that $\mathbf{G}$ is a forcing that we must define. We choose to make $\mathbf{G}$ time independent. If the matrices $\mathbf{L}$ and $\mathbf{Q}$ represent dynamical laws, then $\mathbf{G}$ replaces all the paramerisations found in GCMs together with the external forcing. We will use observations to specify $\mathbf{G}$. The modal perturbation studies of the previous chapter (equation 3.5) effectively use the following definition of $\mathbf{G}$

$$\mathbf{G} = -\mathbf{L}\overline{\mathbf{\Phi}} - \overline{\mathbf{\Phi}}^\dagger \mathbf{Q}\overline{\mathbf{\Phi}}, \tag{4.2}$$

which is calculated by running the model one timestep forwards from a climatological mean initial condition. The eddy budget equation (3.4) shows that this is the same as

$$\mathbf{G} = \overline{\mathbf{F}} + \overline{\mathbf{\Phi}'^\dagger \mathbf{Q}\mathbf{\Phi}'}. \tag{4.3}$$

Here we see the physical meaning for this specification of $\mathbf{G}$. It represents all the processes that are necessary to maintain the time mean circulation against its own advective tendencies. These processes are time mean diabatic forcing, and transient eddy forcing. This last term in (4.3) represents the feedback of the transient perturbations on the mean flow. Recalling our philosophical problems from the last chapter, if this term is included in the forcing, the process can not also be explicitly represented in the model. For transients to be explicit in the model we need to subtract this term, and define $\mathbf{G}$ instead as

$$\mathbf{G} = \overline{\mathbf{F}} = -\mathbf{L}\overline{\mathbf{\Phi}} - \overline{\mathbf{\Phi}^\dagger \mathbf{Q}\mathbf{\Phi}}, \tag{4.4}$$

which in fact is obvious from a comparison of (1.1) and (4.1), but breaking down the meaning of the forcing into its components eases comparison with simpler models presented later. Now $\mathbf{G}$ represents diabatic forcing only, the terms which are usually parameterised in full GCMs. This forcing can also be calculated from the observed timeseries of $\mathbf{\Phi}$, again by running the model for one timestep, but now this must be done more than once. The the results presented below

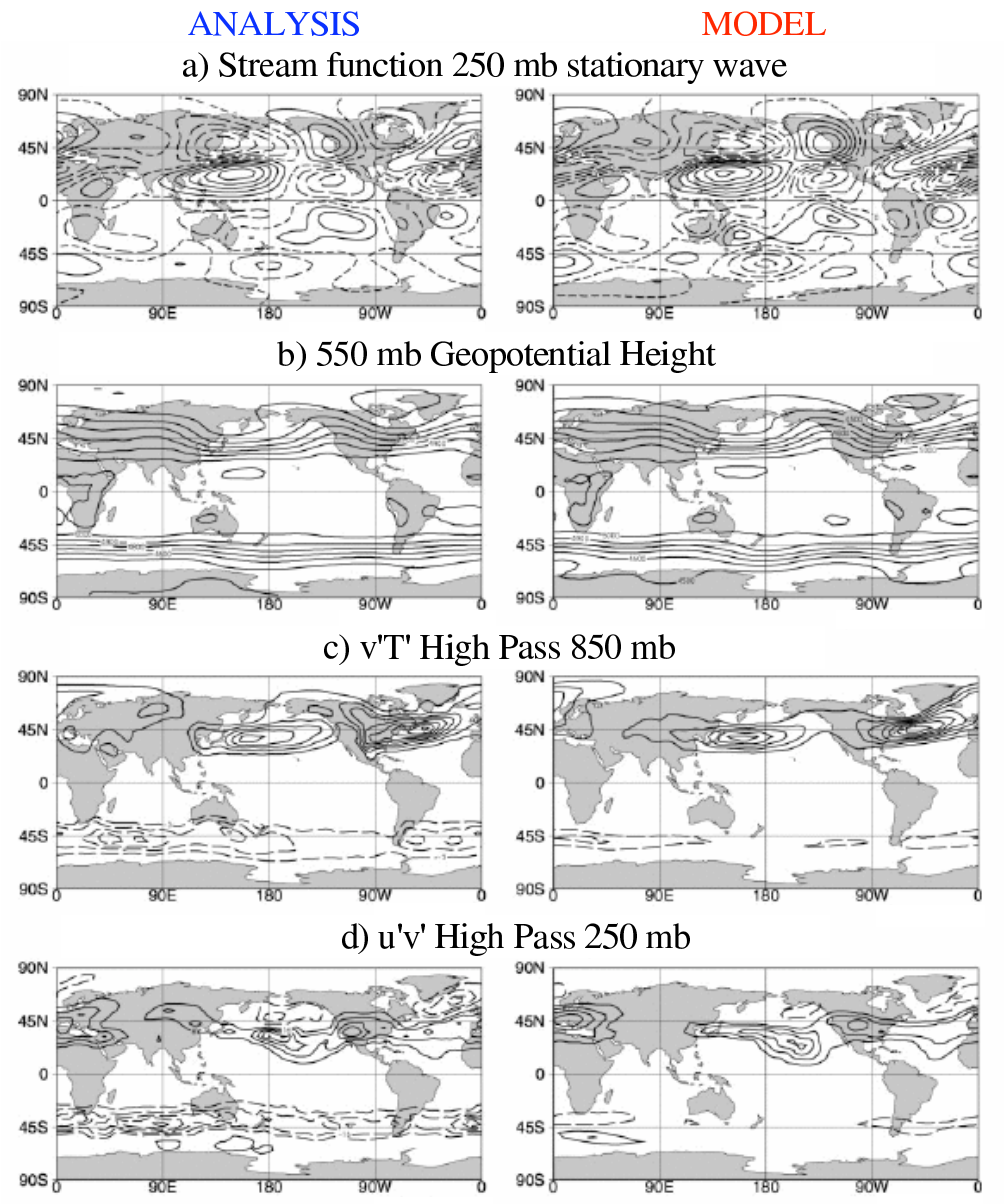

Figure 4.1. *Selected diagnostics from a 9-year winter climatology of ECMWF analyses (left) and from the simple GCM model (right). (a) 250 mb streamfunction (zonal mean removed), contours* $5 \times 10^6 m^2 s^{-1}$. *(b) 550 mb geopotential height, contours 100 m. (c) 850 mb transient northward temperature flux (filtered < 6 days), contours 3 K m* s^{-1}. *(d) Filtered 250 mb transient northward flux of westerly momentum, contours* $8 m^2 s^{-2}$. *Negative contours dashed.*

come from a simple GCM in which ten years of daily data were used to initialise an unforced primitive equation model, and **G** is the negative average of all these one-timestep tendencies (another way of looking at **G** is as the forcing needed to remove the systematic error from a series of one timestep forecasts with an unforced dynamical model). The fact that the forcing has been specified empirically from observations does not guarantee that the model will produce

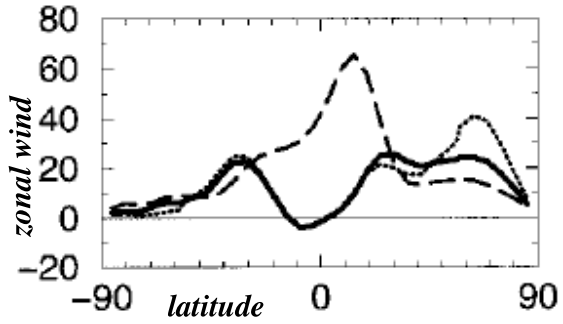

Figure 4.2. *100 mb zonal mean zonal wind showing sensitivity of simple GCM to drag coefficient in the lowest layer. Solid line - timescale 1 day, dotted line 2 days, dashed line 0.5 days.*

a realistic simulation. The only thing that is guaranteed is that

$$\mathbf{L}\overline{\mathbf{\Psi}} + \overline{\mathbf{\Psi}}^{\dagger}\mathbf{Q}\overline{\mathbf{\Psi}} + \overline{\mathbf{\Psi}'^{\dagger}\mathbf{Q}\mathbf{\Psi}'} = \mathbf{L}\overline{\mathbf{\Phi}} + \overline{\mathbf{\Phi}}^{\dagger}\mathbf{Q}\overline{\mathbf{\Phi}} + \overline{\mathbf{\Phi}'^{\dagger}\mathbf{Q}\mathbf{\Phi}'}. \tag{4.5}$$

There are many ways of satisfying (4.5) with radically different $\mathbf{\Psi}$ and $\mathbf{\Phi}$. In physical terms it is only the total flux in the model that must equal the total observed flux at each point. The partition between the mean flow and transient part of that flux is unconstrained. The model may have large systematic errors and still satisfy this equilibrium constraint.

Another point worthy of mention is the equivalence of this forcing specification to the 'restoration forcing' often used in simpler idealised studies, more typically in zonal channel models. In these studies a state variable is 'restored' linearly towards an equilibrium profile which may be far from any observed or model state. Now $\mathbf{L}$ normally contains some linear damping in addition to the linear terms in the primitive equations, as discussed in the stability studies of the previous chapter. If this damping acts locally (i.e. it is diagonal in $\mathbf{L}$) then our specification is mathematically identical to restoration forcing. The only difference is that we do not specify any restoration profile, but rather we specify the damping timescales and deduce the forcing objectively from data.

An extensive investigation onto the behaviour of this simple GCM was carried out by Hall (2000). It was the first time such a model had been constructed with the primitive equations, with the advantage of a full representation of the tropical divergent circulation and the ability to apply the model to tropical-extratopical interactions. Some results are shown in fig. 4.1. The upper level stationary wave structure and zonal jets are well represented by the model, as is the tropical divergent circulation (not shown). Distributions of high pass filtered transient fluxes also show a satisfactory representation of the storm tracks, at least in the northern hemisphere. Upstream poleward temperature fluxes and downstream convergent momentum fluxes are all well situated. The main systematic error of the model is a failure to produce adequate transient activity in the southern hemisphere. This is linked to a compensating error in the mean meridional wind, so the observed balance between Coriolis force and transient momentum flux convergence in the southern Ferrel cell is not properly simulated. The sensitivity to various tunable dissipation parameters was also explored (Hall, 2000). Fig. 4.2 shows the dependence of the upper level zonal mean zonal wind on low level drag. Too little drag and the jet migrates to the polar stratosphere, too much and it shifts towards the equator.

In the next two sections we will use this model, together with simpler versions of the same model with alternative forcing, to investigate the remote response to El Niño and to midlatitude sea surface temperature anomalies.

4.2. Tropical SSTAs

The remote response to El Niño is the clearest example of an atmospheric teleconnection. A warming in the equatorial eastern Pacific is associated with a displacement of convection from the east to the central Pacific, resulting in a deep latent heating anomaly which drives a modified zonal circulation and an enhanced outflow at upper levels. Divergent flux of vorticity into the subtropics creates a source of Rossby waves which then emanate to midlatitudes where the induced circulation projects strongly onto the PNA pattern, that is a low in the eastern Pacific, a high over North America and a low in the western Atlantic.

Numerous modelling studies of varying complexity have been directed at simulating this response, starting with either a source of vorticity in the subtropics or a source of heat at the equator. The details of the PNA response are sensitive to various factors, such as the background flow at the time when the signal is set up, wave-wave interaction in the response itself and transient eddy feedback. Complex interactions between these factors can be difficult to unravel. Hall and Derome (2000) used the model described above in a number of configurations to study these issues.

The basic perturbation to the thermodynamic equation takes the form of a heating centred on the dateline at the equator. It has a zonal extent of 80^0 and a meridional extent of 25^0, with a cosine squared bell shape dependence on the distance from the centre. At the centre the vertical average heating rate is 5^0C per day, equivalent to 2 cm of precipitation per day, a reasonably strong El Niño event. This is distributed into a deep convective profile with a maximum at 350 mb. In general, if this perturbation is applied to any of the model set-ups described above, it will lead to a difference in the time development of the atmospheric state that can be expressed as

$$\frac{d\mathbf{\Delta}}{dt} = \mathbf{L}\mathbf{\Delta} + \left\{\mathbf{\Psi}^\dagger\mathbf{Q}\mathbf{\Delta} + \mathbf{\Delta}^\dagger\mathbf{Q}\mathbf{\Psi}\right\} + \mathbf{\Delta}^\dagger\mathbf{Q}\mathbf{\Delta} + \mathbf{f}_p, \tag{4.6}$$

where $\mathbf{\Delta}$ is the difference between perturbed and unperturbed experiments and $\mathbf{f}_p$ is the tropical heating anomaly. Note that the term in curly brackets is linear in the response $\mathbf{\Delta}$. If the basic model forcing $\mathbf{G}$ is specified such that the basic state is kept fixed, as for the modal experiments in the previous chapter, then $\mathbf{\Psi}$ in (4.6) is constant, and the only thing that develops is the direct response to the heating, $\mathbf{\Delta}$. If on the other hand $\mathbf{G}$ is specified for a simple GCM as above, $\mathbf{\Psi}$ will develop from any initial condition, and $\mathbf{\Delta}$ then represents a tangent response about an evolving basic state. Either way it is clear that the response will depend on the basic state, and in the latter case on the evolution of the basic state. The way in which $\mathbf{\Psi}$ develops in the tangent case is governed by nonlinear dynamics, so even if a given perturbation experiment is linear in $\mathbf{\Delta}$, some rectification effects may be expected, and the average direct response over a range of initial conditions may differ from the single direct response for the average initial condition of that range. The next term in the equation is nonlinear in $\mathbf{\Delta}$ and represents wave-wave interactions in the direct response. For time dependent basic states this term also contributes the transient eddy feedback.

In the first experiment, a linear perturbation model (fixed basic state) based around the observed wintertime flow is carried out. The result is shown in fig. 4.3 in terms of the 250 mb stationary wave streamfunction anomaly. The initial response is a tropical quadrupole and a Kelvin wave that propagates rapidly eastwards, filling the tropical band within 10 days. A stationary Rossby wave is set up over North America by day 15. After about 20 days the solution gives way to a growing storm track mode like the one in fig. 3.2, that is independent of the initial forcing perturbation. We take the day 15 solution as representative of the direct response to El Niño. It is reproduced in fig. 4.4a in terms of the 550 mb geopotential height anomaly.

Some questions can be asked about this solution. How important is nonlinearity in the case of a time independent basic state ? How sensitive is the solution to the choice of basic state ? Fig 4.4b shows the equivalent nonlinear solution in which the perturbation heating was imposed with finite amplitude. The effect for this observed climatological basic state is slight:

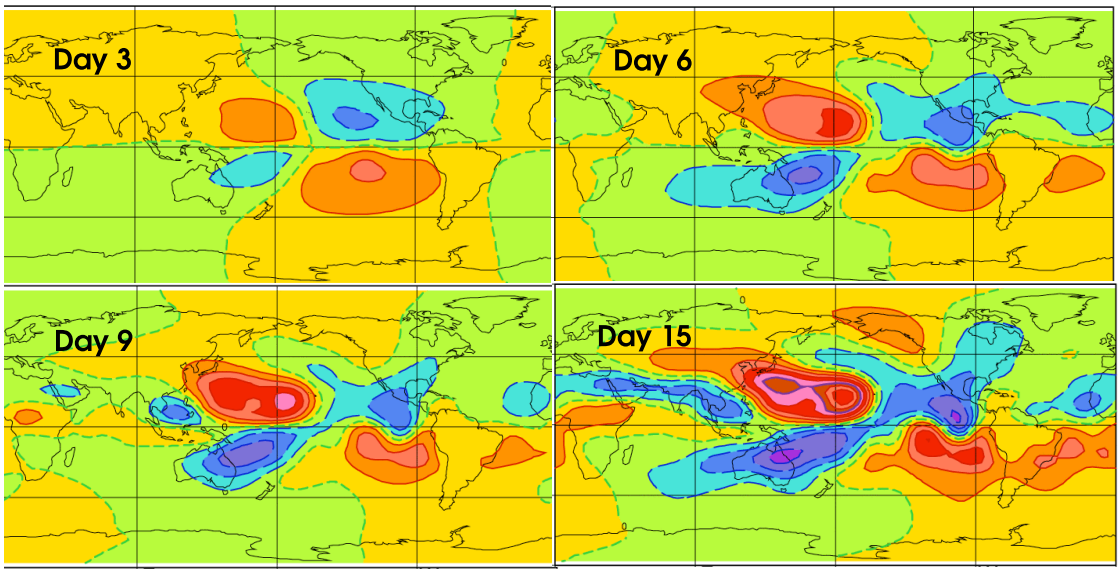

Figure 4.3. *Time dependent linear response to a fixed 'El Niño' heat source on the dateline at the equator with a deep convective vertical profile. Streamfunction anomaly at 250 mb with zonal mean removed. Contours* $2.5 \times 10^6 m^2 s^{-1}$*, negative dashed and green-blue.*

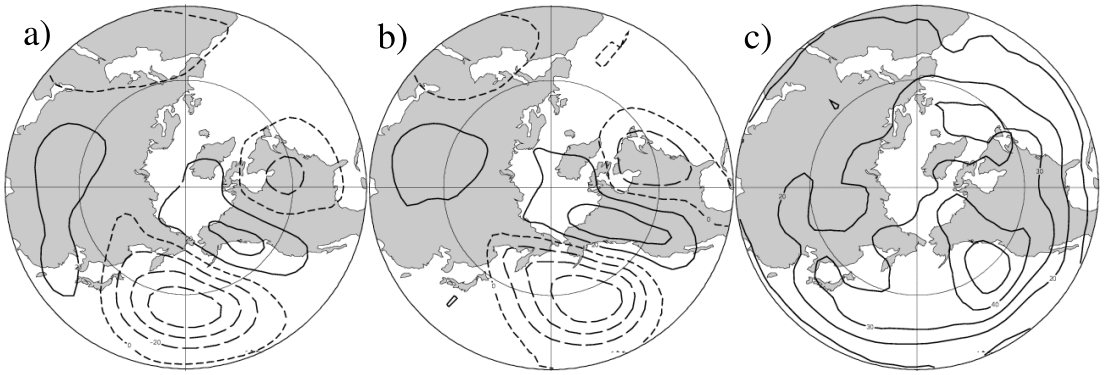

Figure 4.4. *Day-15 550 mb geopotential height anomalies for time dependent perturbation experiments with a fixed equatorial heat source and an observed climatological basic state. (a) linear response. (b) nonlinear response (full amplitude heating). (c) standard deviation for an ensemble of 54 different observed basic states. Contours 20 m (a and b), 10 m (c), negative dashed.*

with some amplification and eastward shift of the high centre. This effect is reproduced for an ensemble of observed basic states (not shown). Fig 4.4c shows the standard deviation of the day 15 solution over 54 different basic states based on 15-day averages from the observational dataset. The variations in the solution are of the same order as the solution itself, implying a strong dependence on observable differences in the basic state during the setup time.

We now turn our attention to tangent experiments, in which the basic forcing $\mathbf{G}$ is specified to give a simple GCM. Thus the unperturbed model integration now develops in time ($\mathbf{\Psi}$ is no longer fixed in (4.6)) and the perturbed integration develops slightly differently. Fig 4.5a shows the tangent linear response using the simple GCMs own time mean climatology as an initial condition. Clearly there is a lot more amplitude in this response, which appears much

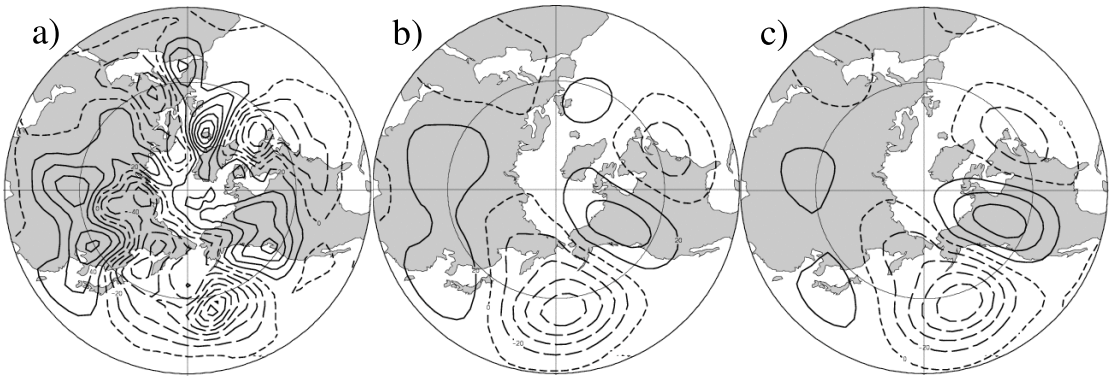

Figure 4.5. *Day-15 550 mb geopotential height anomalies for time dependent tangent perturbation experiments about a time-developing basic state. (a) single linear experiment with simple GCM mean state as initial condition. (b) ensemble mean linear result from 700 experiments with initial conditions taken from individual days in a long unperturbed integration of the simple GCM. (c) as (b) but nonlinear response (finite amplitude heating). Contours 20 m, negative dashed.*

more noisy. This response is still linear in Delta, but the rapidly shifting basic state has had a considerable effect. The immediate question is whether this effect is systematic. To answer this question, another ensemble of experiments was carried out, this time with 700 different initial conditions all taken from an independent run of the simple GCM (the GCM was used to provide its own initial conditions to eliminate any drift in the ensemble mean basic state for the 15-day runs). The ensemble mean tangent linear result is shown in fig 4.5b. It is slightly different from an equivalent fixed basic state response experiment based on the model climatology (not shown), but it seems that the aggregate effect of a time dependent basic state essentially cancels out over a large number of realisations, even though it can obviously be important for a given case. When the same ensemble experiment is repeated in the nonlinear case (finite amplitude heating) the difference is significant, as shown in fig. 4.5c. Transient eddy feedback is now allowed to act within the 15-day time frame of the experiment, and it is already making a difference. The high has been significantly amplified.

It remains to examine the sensitivity at equilibrium. The setup of the El Niño response is of interest, but El Niño events last longer than the 15-day setup time. We therefore look at the difference between two long runs with the simple GCM, one with the finite amplitude heating anomaly and one without. This is shown in fig. 4.6. Another experiment with an equal and opposite cooling (La Niña) is also shown. Transient eddy feedback in the GCM has further amplified the high over North America. Another feature of the longer run is that there has been time to set up more remote responses over Europe, a feature that is purely driven by fluxes associated with transient systems. Looking at the the La Niña response we see that it is by no means equal and opposite to the El Niño response. The central node over North America (now a low) has nearly disappeared. This asymmetry is another feature of the nonlinearity of atmospheric dynamics mentioned in the introduction.

In summary, we have found, by using the model in various configurations, that the remote response to El Niño is very sensitive to the basic state. On a case by case basis it is also sensitive to time development in the background flow, but this does not create an aggregate effect in large ensembles. Nonlinear self-interaction of the direct response has a small effect, giving a slight eastward shift. Nonlinear transient feedback has a large effect, amplifying the high centre over North America.

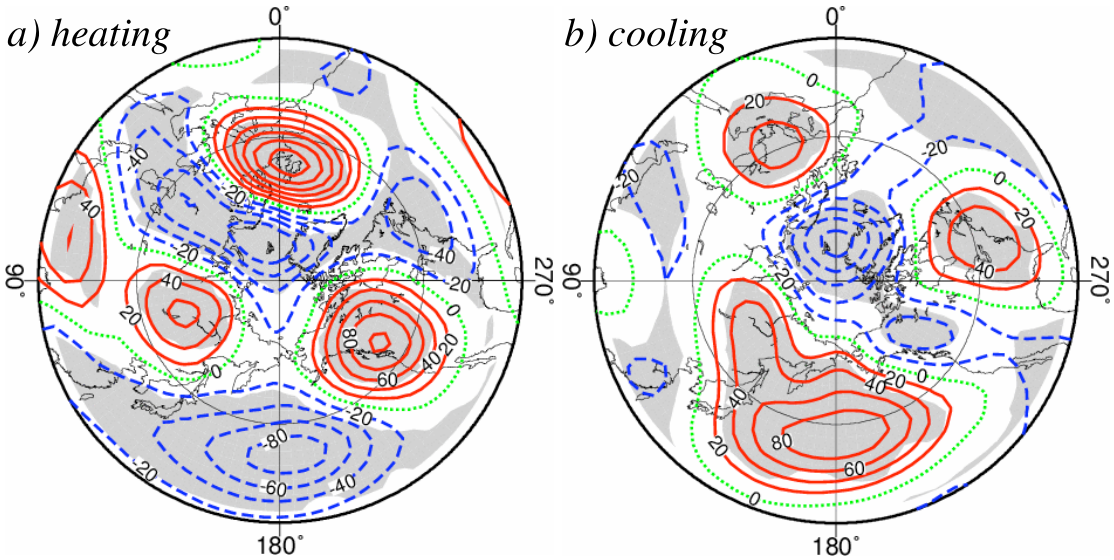

Figure 4.6. *Anomaly in mean 550-mb height (perturbed - unperturbed experiments) for long integrations of the simple GCM : (a) fixed equatorial heating, (b) an equal and opposite cooling. Contours 20 m, negative dashed and blue. Shaded areas indicate where the response is statistically significant at the 99% level according to a two-sided t-test on monthly means.*

4.3. Midlatitude SSTAs

The success of theory and models in diagnosing the midlatitude response to tropical SST anomalies leads us to ask whether the same thing can be done for midlatitude SST anomalies. The temperate oceans exhibit large variations in surface temperature on long timescales. Could this be useful for predicting the atmospheric circulation ? In fact the relationship appears to be more complicated, and most of the variance in midlatitude SSTs actually lags behind the coupled variance in the atmosphere. The atmosphere effectively forces the ocean rather than the other way round. However, this does not mean that midlatitude SSTAs contain no information that could be useful for forecasts. The ocean has a longer memory than the atmosphere, and a persistent anomaly might feed back on the circulation providing some forecast skill. With this in mind, many studies have been made with GCMs to look at the atmospheric response both to observed and idealised midlatitude SST anomalies. Unlike the tropical case, there has been a large degree of disagreement between model results. The barotropic / baroclinic nature of the response, and linearity or symmetry with respect to surface heating and cooling seem to be quite model dependent. The reason for this is most likely to be related to each GCMs differing simulation of the climate and its transient disturbances. The interaction of the SSTA with the climatological jets and storm tracks determines the response. Such things as nonlinearity, or sensitivity to numerous factors can be difficult to diagnose in a GCM, and the problem is quite amenable to the diagnostic modelling treatment discussed here. With the midlatitude problem an equilibrium approach is more appropriate than the transient set-up problem studied in the previous section. Hall *et al* (2001a) simulated a north Pacific SSTA in an equilibrium setting using the simple GCM and the perturbation model as before.

Two long integrations with the simple GCM were carried out, one with a heating perturbation $\mathbf{f}_p$ and one without. If the difference between the two experiments (perturbed minus unperturbed) is $\boldsymbol{\Delta}$, the time mean of (4.6) at equilibrium gives

$$\mathbf{L}\overline{\boldsymbol{\Delta}} + \left\{\overline{\boldsymbol{\Psi}^\dagger \mathbf{Q} \boldsymbol{\Delta}} + \overline{\boldsymbol{\Delta}^\dagger \mathbf{Q} \boldsymbol{\Psi}}\right\} + \overline{\boldsymbol{\Delta}^\dagger \mathbf{Q} \boldsymbol{\Delta}} + \mathbf{f}_p = 0. \tag{4.7}$$

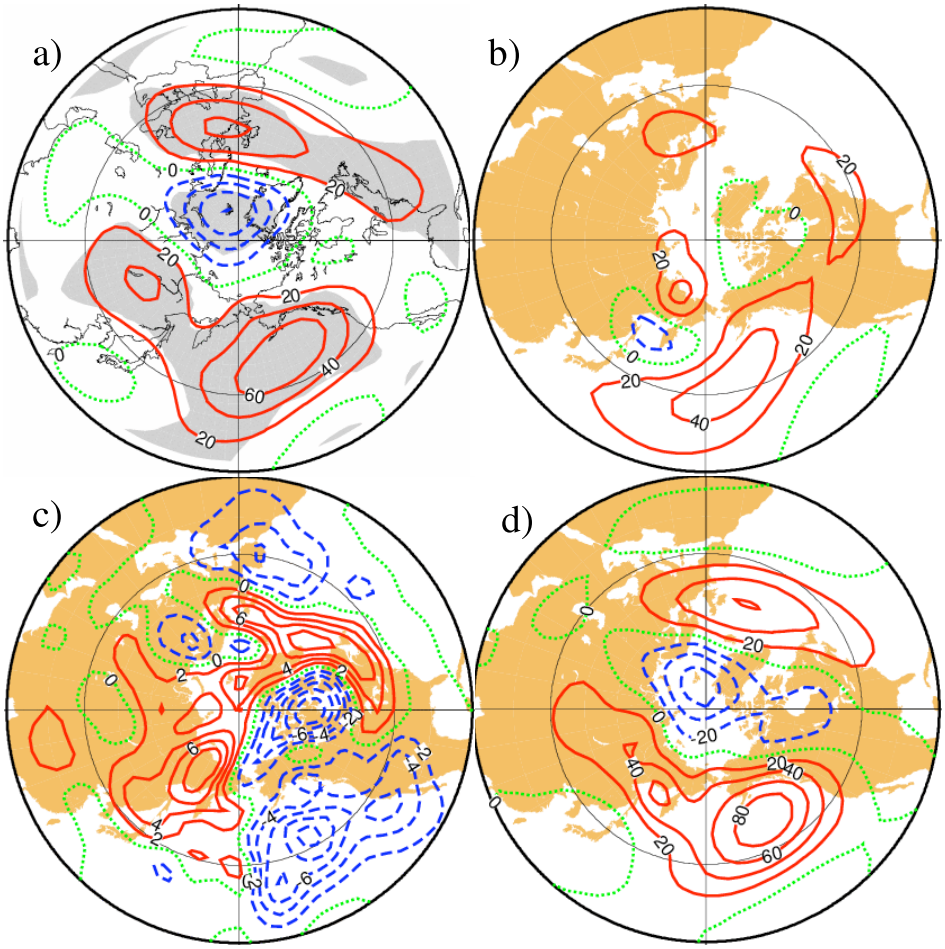

Figure 4.7. *(a) Equilibrium 550-mb geopotential height response of the simple GCM to a fixed shallow heat source in the eastern midlatitude Pacific. Shaded areas show significance as in fig. 4.6. (b) Time independent linear response to the same heat source. (c) Geostrophic source of 550-mb height due to anomalous transient eddies in response to the heating, calculated as* $f/g\nabla^{-2}\{$*transient vorticity flux convergence*$\}$*. (d) Time independent linear response to heating plus transients. Contours 20 m (a,b,d), 2 m per day (c), negative dashed and blue.*

Again the first two terms are linear in $\mathbf{\Delta}$, but now it is clear that the second term depends not only on the control climatology, but also on its mean transients and how they interact with the response. Equation (4.7) can be rewritten

$$-\left\{\mathbf{L}\overline{\mathbf{\Delta}}+\overline{\mathbf{\Psi}}^{\dagger}\mathbf{Q}\overline{\mathbf{\Delta}}+\overline{\mathbf{\Delta}}^{\dagger}\mathbf{Q}\overline{\mathbf{\Psi}}\right\}-\overline{\mathbf{\Delta}}^{\dagger}\mathbf{Q}\overline{\mathbf{\Delta}}=\left\{\overline{\mathbf{\Psi}'^{\dagger}\mathbf{Q}\mathbf{\Delta}'}+\overline{\mathbf{\Delta}'^{\dagger}\mathbf{Q}\mathbf{\Psi}'}+\overline{\mathbf{\Delta}'^{\dagger}\mathbf{Q}\mathbf{\Delta}'}\right\}+\mathbf{f}_p. \qquad (4.8)$$

The term in curly brackets on the left is now linear in the time mean climatologies of the two runs. The second term is the stationary nonlinearity: the self interaction of the time mean response. The curly brackets on the right hand side contain all the effects of the transients. This is more simply expressed as $-\{\overline{\mathbf{\Psi}_p'^{\dagger}\mathbf{Q}\mathbf{\Psi}_p'}-\overline{\mathbf{\Psi}_c'^{\dagger}\mathbf{Q}\mathbf{\Psi}_c'}\}$, where subscripts p and c denote perturbed and control runs. It has been put on the right hand side to emphasise that it can be viewed as a forcing term. Moreover, it is easy to diagnose from the simple GCM results without having to evaluate it directly, because all the other terms in 4.8 concern only the time-means of the two integrations, $\overline{\mathbf{\Psi}}_p$ and $\overline{\mathbf{\Psi}}_c$.

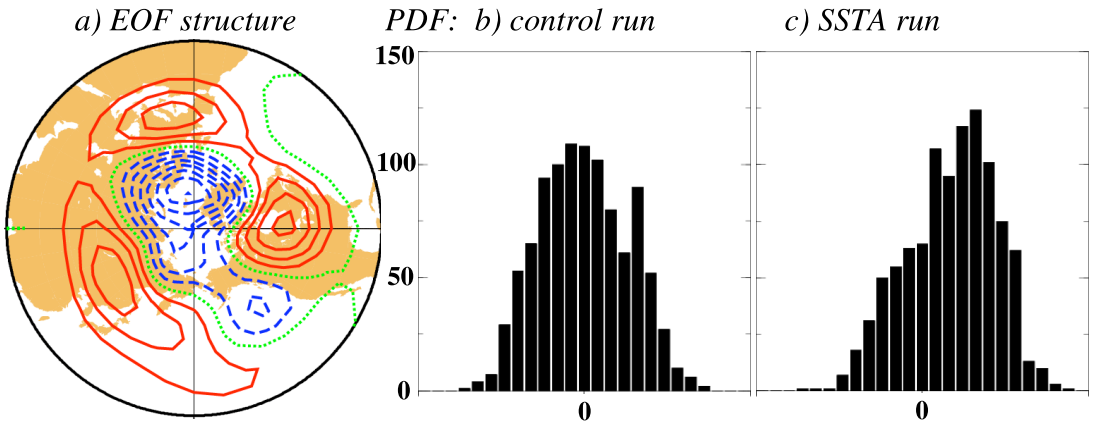

Figure 4.8. *(a) First EOF from monthly mean anomalies for a 1000-month control integration of the simple GCM, explaining 21% of the temporal variance. (b) Probabiliy distribution function of the first EOF. (c) PDF of the same structure projected onto a 1000-month integration with the midlatitude heating perturbation.*

A midlatitude SSTA was simulated by Hall *et al* as a shallow heating perturbation centered on 40^0N, 160^0E with a vertical average central magnitude of 2.5^0C per day, corresponding roughly to an SSTA of 3^0C. The immediate local response to the heating serves to effectively modify it for equilibrium considerations, reducing its amplitude and inducing an effective cooling downstream. The time-mean response to this heating is shown in fig. 4.7 in terms of the 550 mb geopotential height anomaly. The local response is a baroclinic downstream ridge in accordance with quasigeostrophic scaling arguments. There is also an equivalent barotropic remote response in the form of a dipole over Europe. How much of this is attributable to the direct linear response and how much is driven by transients ? To answer this we must solve the time independent linear problem.

If we denote the linear term on on the left hand side of (4.8) as $\mathbf{L}_M\overline{\mathbf{\Delta}}$, ignore the stationary nonlinear term, and consider an unspecified forcing $\mathbf{f}$, the solution for $\overline{\mathbf{\Delta}}$ can be expressed as a sum of eigenmodes of $\mathbf{L}_M$:

$$\Delta_j = -\frac{f_j}{\lambda_j}, \tag{4.9}$$

where f_j is the projection of $\mathbf{f}$ onto the corresponding eigenvector of $\mathbf{L}_M^T$ and λ_j is the jth eigenvalue of $\mathbf{L}_M$. We would like to find this solution without knowing the structure of $\mathbf{L}_M$. If the real parts of all the λ_j are negative, then the system is stable and the problem can be solved by integrating the model with a forcing $\mathbf{G}$ designed to maintain the control climatology $\overline{\mathbf{\Psi}}_c$ as a basic state. With the additional perturbation forcing $\mathbf{f}$ (scaled down to ensure the problem remains linear), the model state will tend towards the steady linear solution $\overline{\mathbf{\Psi}}_c + \overline{\mathbf{\Delta}}$. However, if any of the eigenvalues have positive real parts, this approach will not work. To get around this problem, Hall *et al* used an alternative method in which $\mathbf{L}_M$ is modified with the identity matrix.

We can choose what we want for $\mathbf{f}$. If we choose $\mathbf{f}_p$, then we get the direct linear response to the SSTA. This is shown in fig. 4.7b. Only the local baroclinic part of the solution is present, and with reduced amplitude at upper levels. If on the other hand we choose the entire right hand side of (4.8) for $\mathbf{f}$, we can calculate the linear response to perturbation forcing plus transient feedback. The transient part of the forcing term is shown in fig. 4.7c and the solution in fig. 4.7d. We have now recovered most of the total response. Transients are clearly responsible for the amplification of the response and the European teleconnection. Any remaining difference

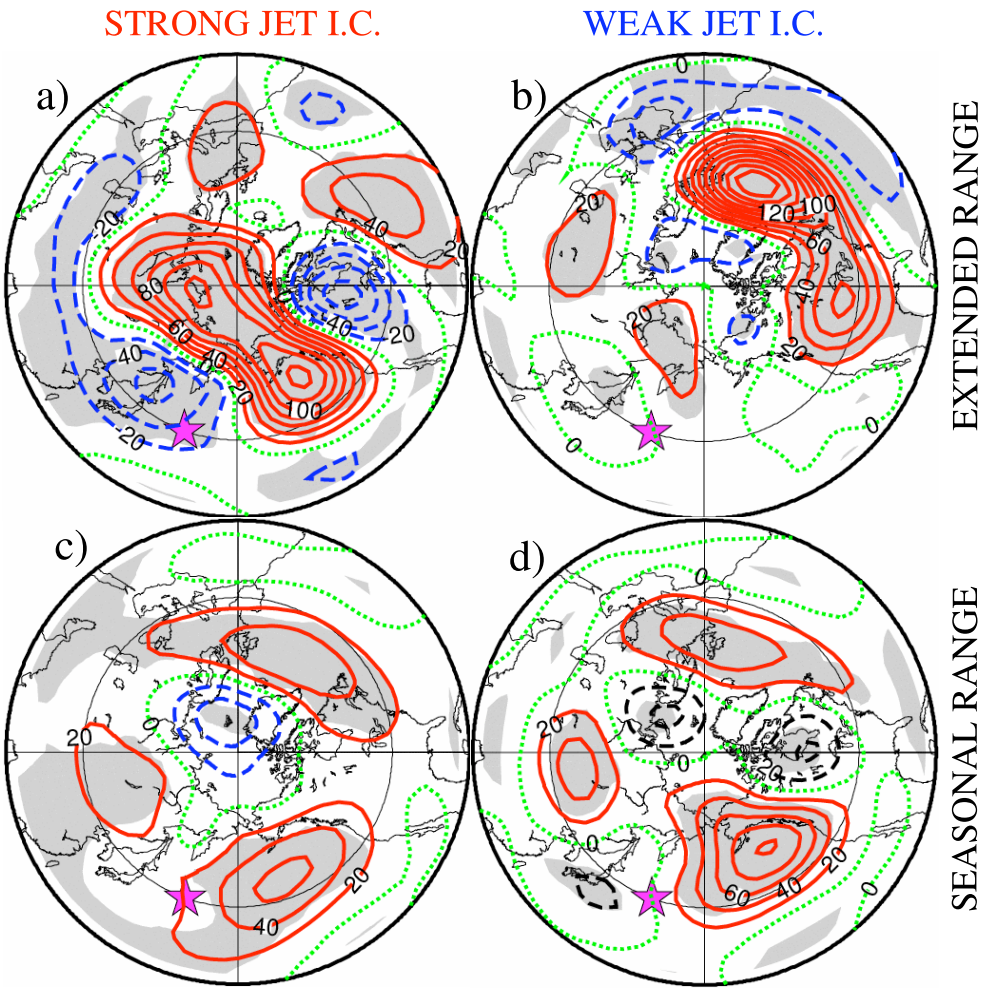

Figure 4.9. *Time development of monthly-mean 550-mb height response to the midlatitude heating. Differences between ensemble means (perturbed - unperturbed) are shown for the extended range (a and b) and the seasonal range (c and d). Experiments with two very different initial conditions: strong pacific jet (a and c) and weak pacific jet (b and d) show sensitivity of forecast anomaly to initial conditions for different forecast ranges. Significance is shaded as in fig. 4.6. Contours 20 m, negative dashed and blue.*

between fig. 4.7 a and d is due to the stationary nonlinearity term.

Since it appears that much of our response is driven by transients, it is interesting to look at the changes in low frequency (greater than monthly timescale) variability, which is also essentially driven by transients. Fig. 4.8 shows the first EOF of monthly means taken from a very long (1000 month) control (unperturbed) integration of the simple GCM. This mode of variability has some features in common with the response to a midlatitude SSTA, especially if the direct linear response is subtracted. Also shown in fig. 4.8 are the frequency distributions of projections onto this mode, first for the control run and then for the perturbed run. The shift in the latter histogram reflects the positive projection of the mean response onto this pattern. There is also a significant skew in the perturbed distribution, indicating that the response to the SSTA takes the form of a preferential occupation of positive phases of this mode of variability

in the perturbed climate.

The presence of a persistent anomaly in the SST, and the fact that the atmosphere may respond to it in a predictable way, has implications for extended range (greater than ten days) and seasonal (greater than a month) forecasts. To test the utility of such an SSTA, Hall *et al* (2001b) performed a large number of ensemble predictions over a range of widely varying initial conditions. Within each 30-member ensemble, small initial perturbations were introduced to make ensemble members diverge from essentially the same large scale flow. This provides for statistically significant results in the extended and seasonal range. Each ensemble experiment was performed twice, once with a heating perturbation and once without, and the influence of the SSTA was then assessed by looking at the ensemble mean response in the extended and seasonal range. The influence of the widely varying initial conditions across the different ensemble experiments was then studied. An illustrative example of the results is shown in fig. 4.9. Two experiments are shown, one with an unusually strong pacific jet, the other with an unusually weak one. In the extended range (forecast month 2) the same SSTA gives a totally different response depending on the initial condition. In the seasonal range (forecast month 3) the responses converge, and start to resemble the equilibrium response studied above. This effect was noted over the whole range of initial conditions studied. The effect of a boundary anomaly is more uniform in the longer range (even though the actual signal might still be weaker). A linear analysis of the variance of the initial conditions versus the responses in the extended range showed that it was extremely difficult to attribute any systematic feature of the response to any systematic feature of the initial condition, limiting the utility of boundary anomalies for forecasting in this range.

5. TRANSIENT DISTURBANCES AND CLIMATE CHANGE

5.1. Global warming

Long term changes in climate are brought about by changes in radiative forcing, which in turn depend on the orbit of the earth and the chemical composition of the atmosphere. In this chapter we will examine various different climates, focusing on the implications of the climate change for the behaviour of transient systems in the atmosphere. We start with global warming, which is the the most rapid climate change ever observed, the effects of which are beginning to be felt. Early GCM calculations of global warming were carried out with a rather academic experiment, to double the amount of CO_2 in the atmosphere in an equilibrium setting. To achieve this the ocean was not allowed to develop, its horizontal fluxes were held constant and the SST was determined with a simple thermodynamic 'slab' upper layer. Recent GCM experiments are more sophisticated, coupled with ocean models and with a range of emission 'scenarios' governing the prescription of CO_2, which changes during the course of a long integration.

Early diagnostics from GCM studies concentrated mainly on average changes in temperature and precipitation. Some of the results were quite reproducible from one model to another. The warming is normally strongest at high latitudes in winter, weakening average midlatitude temperature gradients. Global warming also implies global moistening, with specific humidity increasing fairly uniformly. As model resolution became adequate to simulate midlatitude systems, Hall *et al* (1994) were among the first to study the effects of these climate changes on transient disturbances (this is by far my most cited paper !). The UK Hadley Centre equilibrium 2xCO_2 experiment was diagnosed for changes in many quantities related to midlatitude transient disturbances. On doubling CO_2 this model shows a general weakening of midlatitude temperature gradients, and a strengthening of surface zonal winds in the Atlantic sector. Possible consequences for transients can be assessed in terms of the theoretical growth rate of the fastest growing Eady wave, defined as

$$\sigma = 0.31 \frac{f}{N} \left| \frac{\partial \mathbf{v}}{\partial z} \right|, \tag{5.1}$$

which depends on the static stability and on the magnitude of the vertical wind shear (i.e. horizontal temperature gradient). This measure is used here as a diagnostic pointing to possible enhancements in storm track activity. The difference between 2CO_2 and control experiments is shown in fig. 5.1a. Both Atlantic and Pacific storm track regions show a northward and downstream shift in the growth rate parameter. Diabatic forcing can also contribute to the growth of transient disturbances, and with increased moisture availability, condensation heating may play a role in invigorating developed weather systems, although this issue is complicated, and is discussed below. Fig. 5.1b shows the total diabatic heating anomaly. The decrease in the western Atlantic is due to reduced sensible heating and the increase in the eastern Atlantic is due to enhanced latent heating. The high pass filtered eddy kinetic energy is shown in fig. 5.1c. The downstream and northward shift suggested by fig. 5.1a is evident, and in the Atlantic there is a particularly strong downstream intensification, possibly linked to changes in diabatic forcing.

The contribution of transient systems to the global energy budget can also change with changing climate. In the present day climate the transients carry a significant part of the northward heat flux in midlatitudes. This is measured through fluxes of the field variables 'dry static energy' = $c_pT+\Phi$ and 'moist static energy' = $c_pT+\Phi+Lq$, where Φ is the geopotential and q is the specific humidity. Zonal mean fluxes of these quantities balance boundary source terms due to radiative and sensible heating and the surface supply of moisture through evaporation. Fig. 5.2a shows the zonal mean vertically integrated latitudinal fluxes of these quantities for the control experiment. The difference between moist and dry static energy contributions shows how important the moisture component is to the budget in this model. The moisture flux adds to the total in midlatitudes, mainly because of transient moisture fluxes. In the tropics the moisture flux opposes the dry static energy flux. This is because the Hadley cell transports

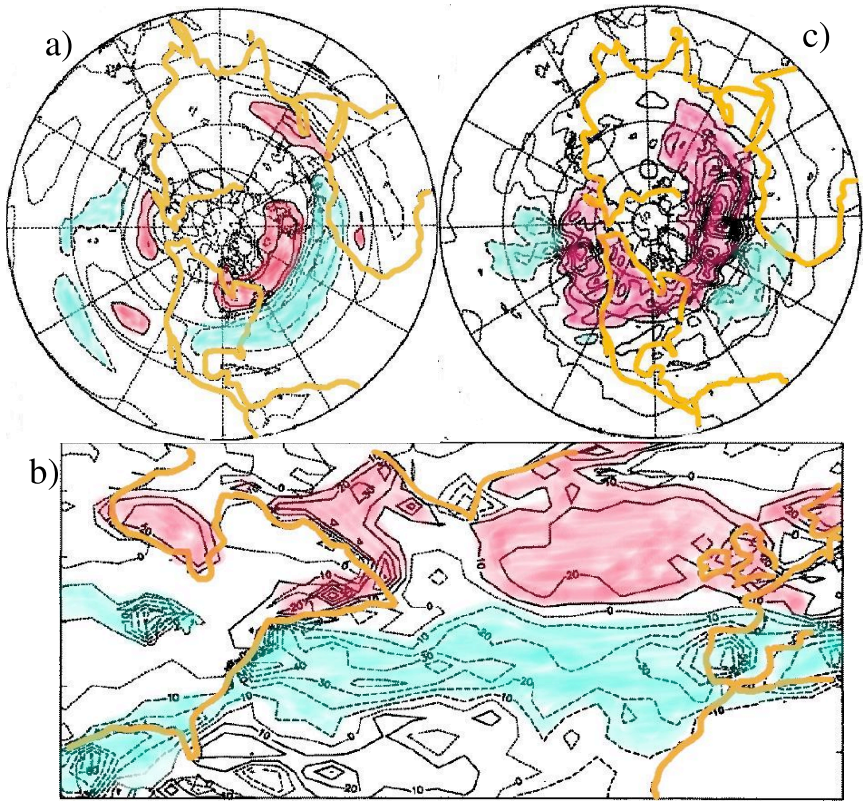

Figure 5.1. *Difference ($2CO_2$ - Control) between equilibrium global warming GCM experiments for (a) Eady growth rate, contours 0.05 days^{-1}, (b) vertically integrated diabatic heating, contours 1 W m^{-2}, (c) high pas filtered 250 mb transient eddy kinetic energy, contours 5m^{2}s^{-2}. Positive/negative areas artistically airbrushed red/blue, negative contours dashed.*

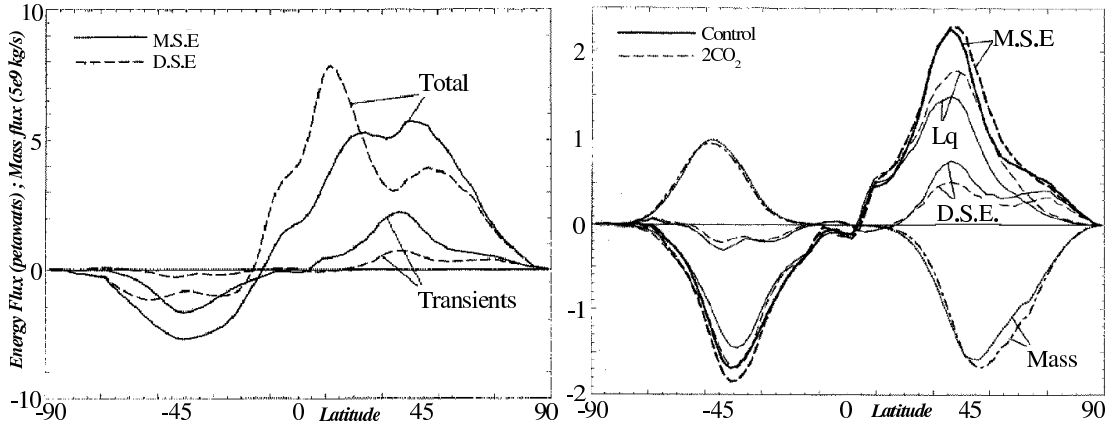

Figure 5.2. *Zonal mean northward flux of moist and dry static energy for the control GCM integration, showing the contribution of the transients, and for the $2CO_2$ integration, showing the changing contibutions of dry and moist components.*

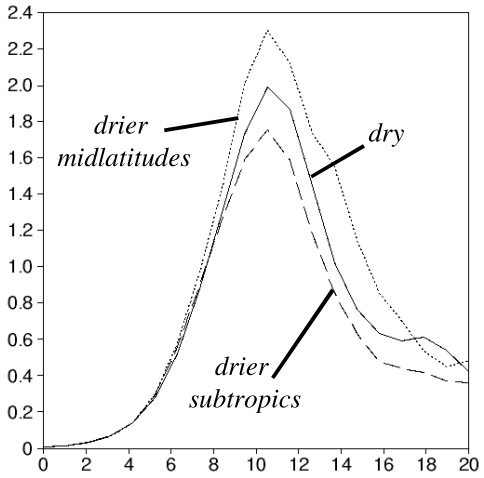

Figure 5.3. *Time development of eddy kinetic energy for three baroclinic wave lifecycle experiments with different initial moisture distributions. Dry (solid curve), moist with relatively dry subtropics (dashed) and moist with relatively dry midlatitudes (dotted). Ordinates 10^5 J m^{-2}, absiscae days.*

moisture towards the equator, into the ITCZ (in fact the Hadley cell also transports heat equatorwards, but the upper level outflow compensates for these effects through the geopotential term). Doubling CO_2 makes very little difference to the transient poleward energy flux (or indeed to the total). The atmospheric component of the energy budget is fully determined by the small change in top-of-the-atmosphere radiation budget, because the oceanic component has been fixed. The partition between time mean and transient components has changed very little. However, the partition between moist and dry components has changed appreciably. In the warmer moister world, the transients are on average less active, but compensate for this by transporting more water vapour. Thus we we see that despite local increases in storminess, the zonal mean reduction in temperature gradients seems to carry through to the zonal mean transient energy budget.

The idea that increased moisture availability might influence the number and intensity of midlatitude systems in a warmer world is worth pursuing. The most important thing to realise is that competing effects are at work. There are ways in which increased humidity can enhance the growth of transients: heating in phase with the temperature wave can give a direct energy boost to a growing system. But latent heating can also inhibit growth: heating in cold air depletes available potential energy, and if water vapour is transported north before it condenses, this reduces the budget requirement for active systems. In a careful set of experiments designed to isolate these effects from other features of climate change (reduced temperature gradients), Pavan *et al* (1999) performed a series of single-eddy lifecycle experiments with a primitive equation model and a simple parameterisation of large scale condensation heating. The zonal mean climate of the GCM control experiment discussed above was used as an initial condition, but the humidity was replaced with various idealised profiles. The profiles were defined in terms of relative humidity in recognition of the fact that this is the appropriate variable to study closeness to saturation, and thereby the potential for latent heating. Observations show that relative humidity decreases smoothly with height but varies considerably with latitude. It is high in the tropics and midlatitudes and low in the subtropics. Experiments which exaggerate or attenuate these effects in the initial condition were carried out to examine the sensitivity of the resulting baroclinic wave. Fig. 5.3 shows three results for the time development of the eddy kinetic energy. The reference experiment is dry. The experiment labelled G100ST60 has

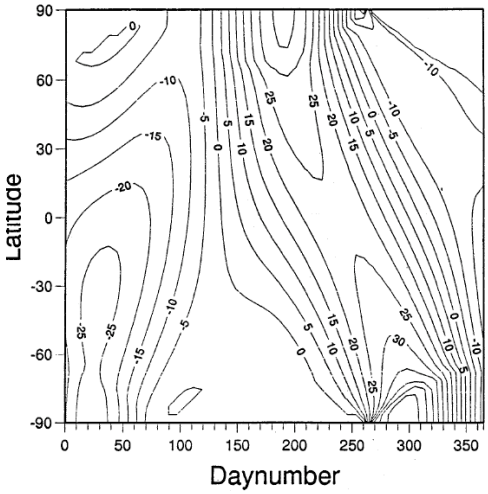

Figure 5.4. *Difference in top of the atmosphere incoming solar radiation between 6000 years ago and the present day (6k - PD). Daynumber from the first of January. Contours 5 W* m^{-2}.

an initial condition with 100% humidity everywhere except the subtropics where it is 60%. The experiment labelled G100ML60 has reduced initial relative humidity in the midlatitudes. It is clear that in the former case the kinetic energy is reduced and in the latter it is enhanced. The conclusion is that more moisture in the subtropics might lead to stronger midlatitude systems but more moisture in the midlatitudes will weaken them. Pavan *et al* explain these results in terms of the energetics of the wave.

Such a simple set of experiments of course neglects many factors, such as non-modal growth of systems and longitudinal variations in relative humidity. But it is interesting to note that a 'most realistic case' would correspond to a 'G90ST80' experiment, which actually shows no change from the dry experiment and lies exactly on the cusp of the sensitivity revealed by these lifecycle experiments. The broad conclusion, then, is that with changes in moisture, it could go either way. Anyone who actually tries to read Pavan *et al* will be bludgeoned into an appreciation that the problem is fiendishly complicated, and will exercise caution before making vacuous statements about how 'more moisture', or 'more energy' will lead to 'bigger storms'. Statements about 'extreme events' based on this kind of reasoning are even more precarious.

5.2. The mid-Holocene

Six thousand years ago, at the dawn of the ancient Egyptian civilisation, the earth's axis of rotation did not point at Polaris, our familiar pole star. It pointed at Thuban, a 3.7th magnitude star 309 light years away in the constellation of Draco. Unbeknownst to the Pharoes, this had implications for the earth's climate, including transient disturbances. The orbit of the Earth can be described by three parameters, the eccentricity of the ellipse, the obliquity (tilt) of the axis and the date of the perihelion, when we are closest to the sun. Presently these parameters are 0.016724, 23.446 deg and 282.04 days from the vernal equinox. Six thousand years ago they were 0.018682, 24.105 deg and 180.87 days. The earth was thus slightly more tilted, and rather than being closest to the sun in mid-winter, it was closest in autumn. The resulting changes to the top-of-the-atmosphere incoming radiation are shown in fig. 5.4. The increased obliquity enhances the seasonal cycle in both hemispheres, and the change in the perihelion date has the effect of extending the northern hemisphere summer, and giving an early start to the southern hemisphere summer.

Two ten-year integrations of the UK UGAMP GCM were carried out by Hall and Valdes

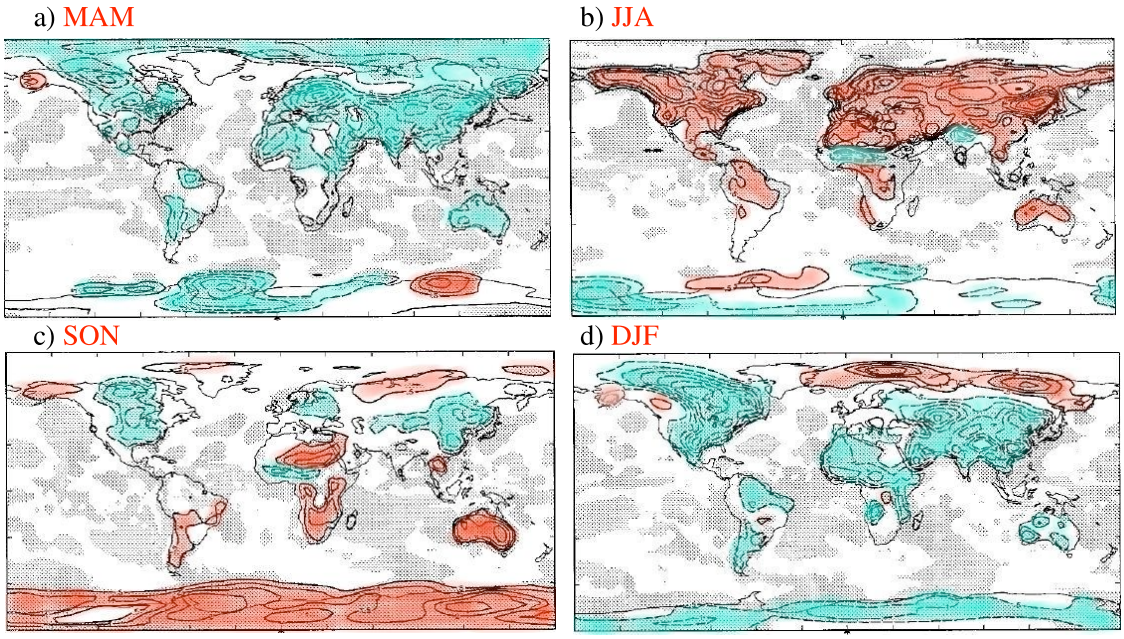

Figure 5.5. *Surface air temperature anomaly (6k - PD) for the four seasons, a) spring, b) summer, c) autumn, d) winter. Contours $0.5^0 C$, red warm blue cold. Stippled areas denote significance at 95% level.*

(1997), for present day and 6k yr climates. They differ only in their orbit and in the CO_2 concentration, which is contemporary (345 ppmv) for the present day and pre-industrial (280 ppmv) for 6k. Sea surface temperatures were fixed to the same value in the two integrations. The change in ten year mean surface temperature is shown in fig. 5.5 for the four seasons. Continental temperature changes are the result of the surface radiation budget, which is determined by the incoming radiation at the top of the atmosphere and the intervention of clouds and changes in surface temperature and albedo (due to snow cover). In general the results shown in fig. 5.5 reflect the orbital perturbation. Spring is cool in the northern hemisphere, but summer is warmer. Summer warmth sweeps southwards to bring early summer to the southern hemisphere.

Changes in continental temperature lead to changes in surface pressure. The thermally direct response is a heat low, with an associated large scale convergent 'monsoon' circulation and enhanced upward motion and precipitation. Changes in horizontal temperature gradients also give rise to changes in jet structure, and this in turn affects the storm tracks and the distribution and intensity of rain-bearing transient weather systems. In the current study this all happens in a very seasonally dependent way, but can nevertheless have consequences for annual mean measures of surface hydrology. Fig. 5.6 shows the annual mean change in precipitation minus evaporation. This figure is dominated by changes in convective activity associated with changes in the position of the ITCZ. Most of these changes take place over the ocean and are thus not amenable to verification against paleoclimatic data, which comes from sources such as lake levels and pollen types. However, some features in the tropics and the midlatitudes do match the observations.

The most striking feature is the enhanced African monsoon. This is a consequence of a much warmer Sahara in summer, leading to an intensified summertime Saharan low, and associated onshore monsoon winds from the Gulf of Guinea, resulting in a wetter Sahel. The northern hemisphere summer continental warming is also generally well verified against paleoclimatic data. The rotational (geostrophic) part of the response also has verifiable consequences. Con-

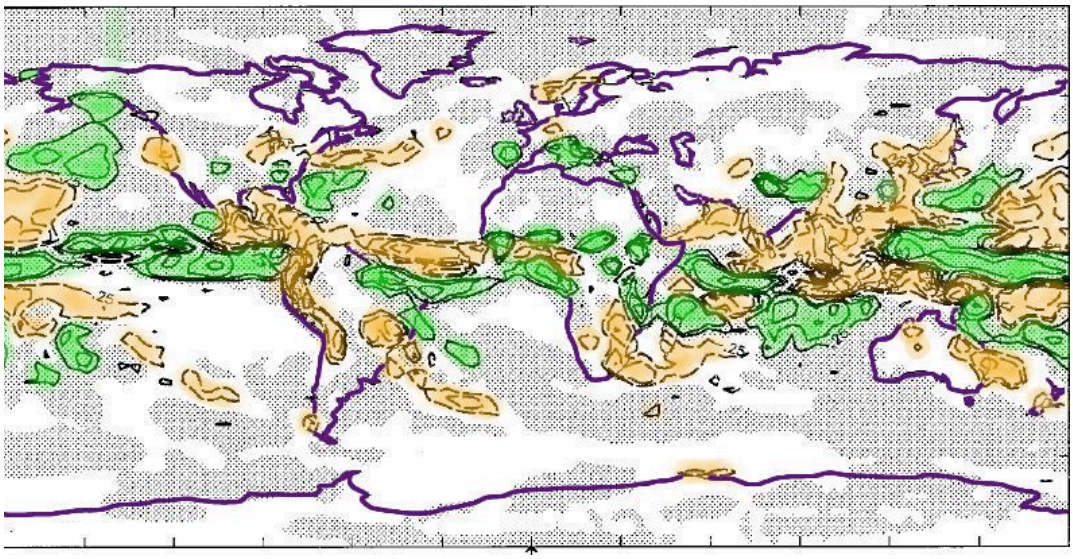

Figure 5.6. *Change (6k - PD) in annual mean surface hydrological budget (precipitation - evaporation). Contours 0.25, 0.5, 1. 2... mm per day. Positive (wet) areas are stippled. Wettest areas shaded green, driest areas shaded brown.*

tinental cooling over North America in the winter results in a westward shift of the Aleutian low, resulting in weaker onshore winds on the west coast. There is an associated reduction in transient activity, and precipitation, resulting in a drier California. Over western Europe, wintertime is wetter for the Mediterranean region, due to increased temperature gradients off the east coast of North America leading to a stronger storm track and increased precipitation, particularly over Iberia.

All these features show up in the annual mean and in the paleoclimatic data. There are other areas where the model gets it wrong, particularly over the Australian continent. Ultimately the precipitation is the end product of a long chain of events, and strong signals are needed, together with corroboration from other models, to attribute significance to model results.

5.3. The last ice age

Twenty one thousand years ago the northern hemisphere continents were covered with mountains of ice. Two species of humans vied for existence, hunting mammoths and fleeing from sabre toothed tigers. They had mastered the use of fire, and were already developing an intuitive appreciation of the role of transient disturbances in the atmosphere. The elevation of the ice sheets is shown in fig 5.7a. According to the CLIMAP reconstruction shown here, the land glaciers over North America and Scandinavia reach up to 3 km and sea ice extends considerably further to the south. This major change in boundary condition has a large effect on the mean temperature simulated with the UGAMP GCM (Hall *et al* 1996). In this model experiment the orbit is again adjusted, but this time the change is not of great importance compared to the change in boundary conditions. CO_2 is also reduced to 190 ppmv. In winter the presence of sea ice causes a cooling in the north Atlantic of up to 20^0C, with an associated increase and sharpening of temperature gradients over the sea ice edge. In the summer there is a similar cooling associated with the radiative balance over the Laurentide glacier. These changes are also shown in fig. 5.7. In what follows we will try to trace the influence of these major perturbations on the circulation, the storm tracks and the precipitation, leading to an assessment of the maintenance of the great ice sheets.

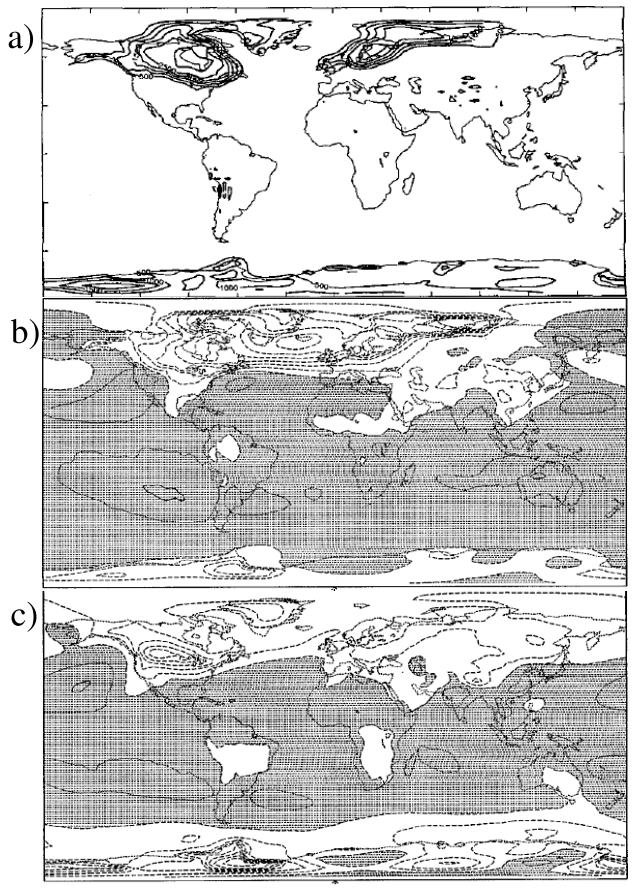

Figure 5.7. *(a) Surface elevation of the glaciers at the last glacial maximum, contours 500 m. (b) Difference (LGM - PD) in 850 mb winter (DJF) temperature. Contours $4^0 C$, positive areas shaded, negative contours dashed. (c) Summer (JJA) temperature difference.*

The response of the mean circulation to these changes in temperature and orography is a strengthening and displacement of the Atlantic jet over the new baroclinic zone to the east, and the appearance of a surface high pressure centre over the Laurentide glacier, bringing more air from the south over the west coast of North America and deflecting the Pacific jet outflow northwards. These changes in circulation and temperature structure can be diagnosed as before in terms of the Eady growth rate. This is shown in fig. 5.8 for a present day simulation and for the last glacial maximum. The dramatic increase in baroclinicity over the north Atlantic can be seen. The baroclinic zone no longer depends on land-sea temperature contrast, but shifts off the continent onto the sea ice edge, migrating north and east. These changes are reflected in the GCMs storm track activity, diagnosed here as the transient northward temperature flux shown in fig 5.9. At the level shown (850 mb) the wintertime Atlantic storm track has greatly intensified and shifted as expected, and the Pacific storm track is also displaced to the east. Also shown in fig. 5.9 is the vertical structure of the zonal mean transient temperature flux. Here we see that although the zonal mean storm track has intensified at low levels, it is also more shallow in the northern hemisphere. The systems that grow on the sea ice edge are smaller in scale both horizontally and vertically, and transport heat over a shorter distance across a narrower zone of large temperature gradients. This observation has implications for the global energy budget, which has been evaluated as before, and is presented in fig. 5.10 for the wintertime

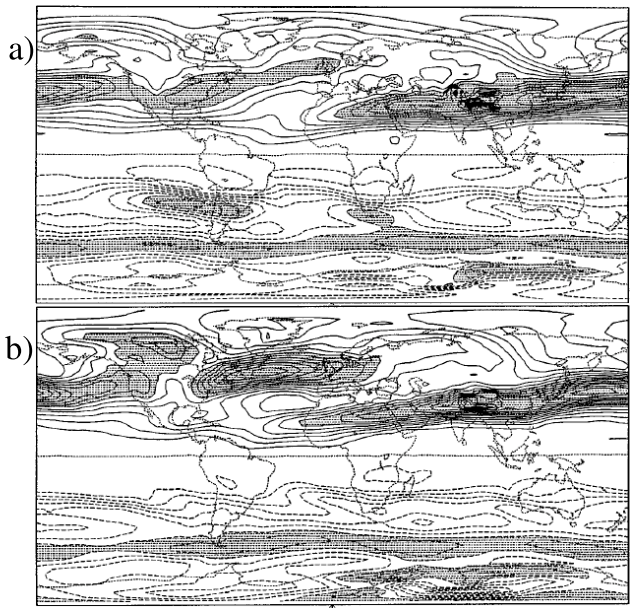

Figure 5.8. *Eady growth rate parameter at 500 mb during winter (DJF) for (a) the present day and (b) the last glacial maximum. Contours 0.1 days^{-1} and shading where the magnitude exceeds 0.6 days^{-1}. Negative contours dashed.*

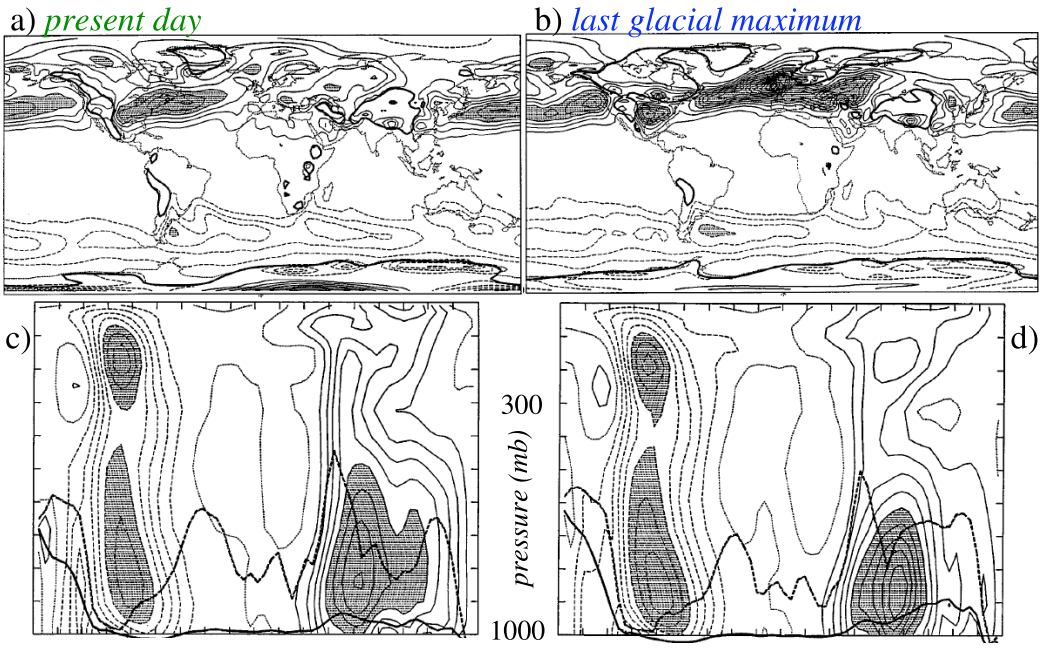

Figure 5.9. *Total transeint eddy temperature flux for (a,c) present day and (b,d) last glacial maximum. (a,b) at 850 mb and (c,d) show zonal mean. Contours 5 K m s^{-1} with shading where magnitude exceeds 20 (a,b) and 2 K m s^{-1} with shading over 10 (c,d). Negative contours dashed.*

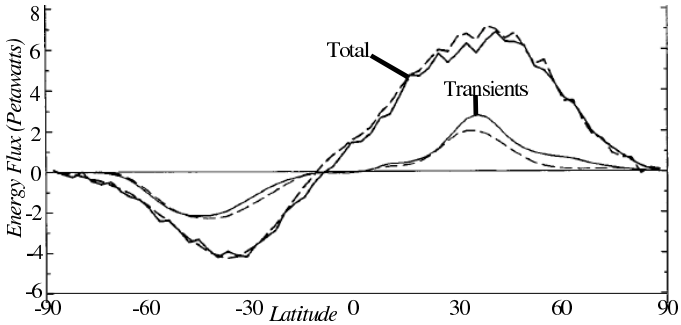

Figure 5.10. *Total vertically integrated cross-latitude flux of moist static energy by the atmospheric circulation during winter (DJF). Total and transient contribution shown for present day (solid) and last glacial maximum (dashed).*

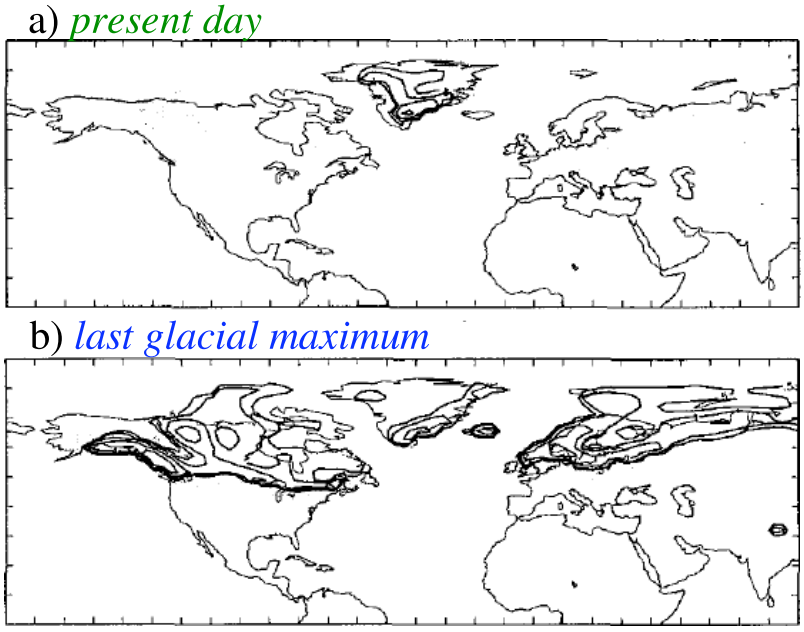

Figure 5.11. *Four-year snow accumulation in m for (a) present day and (b) last glacial maximum. Contours 0.5, 1., 2., ... m. Negative (net ablation) values omitted.*

flow. Despite the dramatic increase in activity in the Atlantic, the transient component of the northward cross-latitude energy flux is actually reduced at the last glacial maximum during winter. In fact there is no increased requirement for northward heat transport in this model, despite the large increase in pole-equator temperature difference. This is because the reduced temperatures at high latitudes imply a reduction in long wave radiation escaping to space in the wintertime, so the radiative imbalance between equator and pole remains about the same.

The increased activity in the Atlantic, and modified circulation in the Pacific have local consequences for precipitation. Western Europe receives more precipitation in the wintertime, as does the western edge of the Laurentide glacier. In the summer, Both Laurentide and

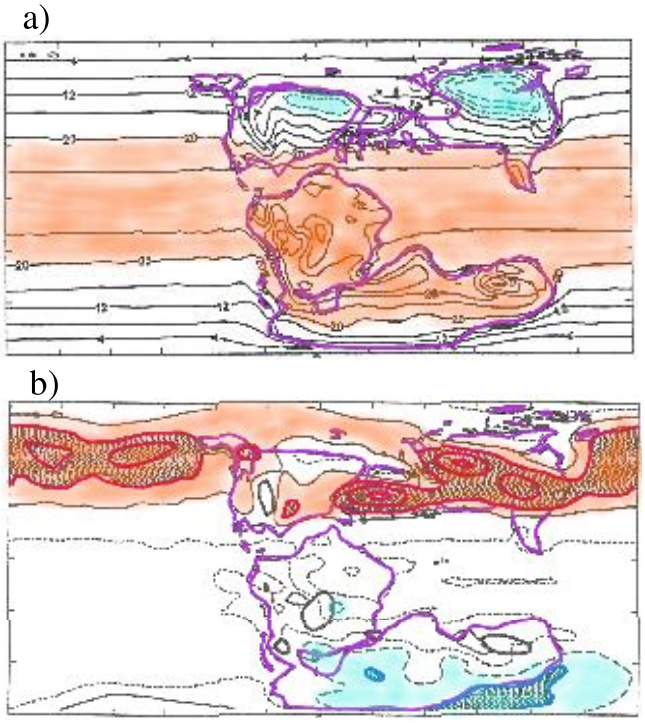

Figure 5.12. *Results from a GCM simulation of the Jurassic. (a) Surface air temperature, contours 4^0C, red above 20, blue below zero. (b) 850 mb high-pass transient eddy northward temperature flux, contours 5 K m s^{-1} (positive/negative red/blue), magnitudes greater than 10 stippled. Negative contours dashed.*

Scandinavian glaciers receive more precipitation in their central regions. Crucially, in the colder climate, a greater proportion of this precipitation falls as snow, and contributes to the mass balance of the glacier. Since the model has a full seasonal cycle, and the accumulation and ablation of snow is simulated, an annual mean measure of net snow accumulation can be obtained. This is shown in fig. 5.11 for the present day and the last glacial maximum. The current climate only maintains a land glacier over Greenland. At the last glacial maximum the two major glaciers show net accumulation at the centre and net ablation at the edges. The rate of accumulation is roughly consistent with the mass balance of a glacier of this size over the timescale for glacier building, although this conclusion is of questionable relevance for a simulation of a glacial maximum, where the glaciers are at a turning point in their evolution. The model is of course unable to make predictions for ice sheet growth and decay, and can only provide forcing at a precise timeslice in history for an ice sheet model. It is nevertheless clear from these experiments that many complex factors must be taken into account when simulating the forcing of the glacial interglacial cycles, including the interaction of glaciers themselves, together with the sea ice, with atmospheric dynamics and the transport of humidity.

5.4. The Jurassic

One hundred and fifty million years ago the dinosaurs ruled the earth. Fearsome creatures with small brains, they had no understanding of transient disturbances. They lived in a world very different from our own with an atmosphere rich in CO_2 (1120 ppmv). The Atlantic Ocean was much smaller as North America and Eurasia had just begun to drift apart, and in the southern hemisphere was the super-continent known as Gondwanaland. The rest of the globe

was covered by the giant ocean Panthalassa. The surface temperature from a GCM simulation of this era is shown in fig. 5.12. SSTs are prescribed as a simple cosine function, but land temperature results from the model's thermal equilibrium and the influence of a reconstructed paleo orography. In this winter season, much of paleo Eurasia is below zero, and there is a zonally extended region of enhanced temperature contrasts to the south. These give rise to a single Jurassic storm track, shown here in terms of the transient temperature flux. The storm track spreads out into Panthalassa, but could easily be modified by the unknown ocean circulation. As well as the storm tracks, the tropical circulation was also very different, with a very intense Hadley circulation and a seasonal change in zonal flow dominated by the Gonwanaland monsoon.

References

Burpee, R.W., 1972: The origin and structure of easterly waves in the lower troposphere of North Africa. *J. Atmos. Sci.,***29**, 77-90.

Charney, J.G., 1947: The dynamics of long waves in a baroclinic westerly current. *J. Meteor.,***4,** 125-162.

Eady, E.T., 1949: Long waves and cyclone waves *Tellus,***1,** 33-52.

Farrell, B.F., 1982: The initial growth of disturbances in a baroclinic flow. *J. Atmos. Sci.,***39,** 1663-1686.

Fofonoff, N. P., 1954: Steady flow in a frictionless homogeneous ocean. *J. Mar. Res.,* **13,** 254-262.

Gent, P.R. and J.C. McWilliams, 1990: Isopycnal mixing in ocean circulation models. J. Phys. Oceanogr 20, 150-155.

Hall, N.M.J., 1991: Depth dependence and mass transport of recirculating mid-latitude gyres. *J. Phys. Oceanogr.* **21**, 824-842.

Hall, N.M.J., 2000: A simple GCM based on dry dynamics and constant forcing. *J. Atmos. Sci.,***57**, 1557-1572.

Hall, N.M.J., 2004: Parameterisation of sub-grid scale turbulence in ocean models. *Final Report, SHOM/UBO contract*, 7pp.

Hall, N.M.J., B. Barnier, T. Penduff and J-M. Molines, 2004: Interannual variation of Gulf Stream heat transport in a high resolution model forced by reanalysis data. *Climate Dynamics* **23**, 341-351.

Hall, N.M.J. and J. Derome, 2000: Transience, nonlinearity and eddy feedback in the remote response to El Niño. *J. Atmos. Sci.,***57**, 3992-4007.

Hall, N.M.J., J. Derome and H. Lin, 2001a: The extratropical signal generated by a midlatitude SST anomaly. Part 1: Sensitivity at equilibrium. *J. Climate,***14**, 2035-2053.

Hall, N.M.J., B. Dong and P.J. Valdes, 1996: Atmospheric equilibrium, instability and energy transport at the last glacial maximum. *Climate Dynamics,* **12**, 497-511.

Hall, N.M.J., B.J. Hoskins, P.J. Valdes and C.A. Senior, 1994: Storm tracks in a high resolution GCM with doubled carbon dioxide. *Quart. J. Roy. Meteorol. Soc.* **120**, 1209-1230.

Hall, N.M.J., G.N. Kiladis and C.D. Thorncroft, 2006: A new perspective on African easterly waves. Part II: Dynamics. *J. Atmos. Sci.,* accepted

Hall, N.M.J., H. Lin and J. Derome, 2001b: The extratropical signal generated by a midlatitude SST anomaly. Part 2: Influence on seasonal forecasts. *J. Climate,***14**, 2696-2709.

Hall, N.M.J. and P.D. Sardeshmukh, 1998: Is the time mean Northern Hemisphere flow baroclinically unstable ? *J. Atmos. Sci.,* **55**, 41-56.

Hall, N.M.J. and P.J. Valdes, 1997: A GCM simulation of the climate 6000 years ago. *J. Climate,* **10**, 3-17.

Hall, N.M.J., P.J. Valdes and B. Dong, 1996: The maintenance of the last great ice sheets: A UGAMP GCM study. *J. Climate,* **9**, 1004-1019.

Pavan, V., N.M.J. Hall, P.J. Valdes and M. Blackburn, 1999: The importance of moisture distribution for the growth and energetics of mid-latitude systems. *Annales Geophysicae,* **17**, 242-256.

Reed, R.J., D.C. Norquist and E.E. Recker, 1977: The structure and properties of African wave disturbances as observed during Phase III of GATE. *Mon. Wea. Rev.,***105**, 317-333.

Rhines, P. B., and W. R. Young, 1982: A theory of the wind driven ocean circulation I.: Mid-ocean gyres. *J. Mar. Res.,* **40**(suppl), 559-596.

Kiladis, G.N., C.D. Thorncroft and N.M.J. Hall, 2006: A new perspective on African easterly waves. Part I: Observations. *J. Atmos. Sci.,* accepted

Treguier A-M., B. Barnier, A. de Miranda, J-M. Molines, N. Grima, M. Imbard, G. Madec, C. Messager and S. Michel, 2001: An eddy permitting model of the Atlantic circulation: evaluating open boundary conditions. J. Geophys. res. 106: 22,115-22,129